MRO FTT/NAS & FLC

FTT/NAS Conceptual Design Report

MRO-TRE-CAM-0000-0102

The Cambridge FTT Team

rev 1.1
31 August 2010

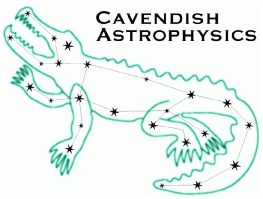

Cavendish Laboratory
Madingley Road
Cambridge CB3 0HE
UK

Change Record

Revision	Date	Author(s)	Changes
0.1	2010-08-20	JSY	Initial version with majority of content
0.2	2010-08-23	JSY	Added software section, last part of layout section
0.3	2010-08-24	JSY	Merged in changes from EBS, MF
0.4	2010-08-26	JSY	Version from CAH plus Appendices. Also minor corrections
0.5	2010-08-27	MF	Additions to appendices and minor changes throughout
0.6	2010-08-27	JSY	Replaced beam train figure, new layouts figure, added equations to appendix
0.7	2010-08-28	CAH	Corrected Table 1, added dichroic section and minor edits throughout
0.8	2010-08-29	MF	Some minor corrections. Revision of appendices
0.9	2010-08-30	MF & CAH	Minor revisions
1.0	2010-08-31	JSY	Minor revisions and formatting corrections
1.1	2010-08-31	JSY	Correction to Appendix B.2. Added paragraph to 9.3.1

Objective

This document presents the conceptual design of the FTT/NA system.

Scope

All aspects of the conceptual design of the FTT/NAS are described in this document. The conceptual design of the FLC is outlined in a separate report (AD1).

Reference Documents

RD1 Technical Requirements: Fast Tip-Tilt/Narrow-field Acquisition System (INT-403-ENG-0003) – rev 2.2, May 20th 2010

RD2 Derived Requirements (MRO-TRE-CAM-0000-0101)

RD3 Technical Requirements: Unit Telescopes for the MRO Interferometer (INT-403-TSP-0003) – October 27th 2006

RD4 ICD List and Expected Content (MRO-LIS-CAM-0000-0107)

RD5 FTT/NAS Requirements Compliance Matrix (MRO-TRE-CAM-0000-0104)

Applicable Documents

AD1 FLC Conceptual Design Report (MRO-TRE-CAM-0000-0103)

AD2 Technical Requirements: First Light Camera (INT-403-TSP-0107) – rev 1.0, May 20th 2010

Acronyms and Abbreviations

AAS Automated Alignment System
ADC Atmospheric Dispersion Corrector
AGN Active Galactic Nucleus
AMOS Advanced Mechanical and Optical Systems (UTM vendor)
BCF Beam Combining Facility
CCD Charge-Coupled Device
CoDR Conceptual Design Review
COTS Commercial Off-The-Shelf
CPU Central Processing Unit
CTE Coefficient of Thermal Expansion
DLT Dog-Leg Transmissive (layout)
DMA Direct Memory Access
DT Direct Transmissive (layout)
EIE European Industrial Engineering (UTE vendor)
EMCCD Electron-Multiplying Charge Coupled Device
FEA Finite-Element Analysis
FTT Fast Tip-Tilt
FLC First Light Camera
FOV Field-of-View
FPGA Field-Programmable Gate Array
FTTA Fast Tip-Tilt Actuator
GUI Graphical User Interface
ICD Interface Control Document
ISS Interferometer Supervisory System
MROI Magdalena Ridge Observatory Interferometer
NAS Narrow-field Acquisition System
NMT New Mexico Tech
OAP Off-Axis Paraboloid
PC Personal Computer
PCI Peripheral Component Interconnect
PDR Preliminary Design Review
PSF Point-Spread Function
ROM Rough Order of Magnitude
RTOS Real-Time Operating System
TBC To be confirmed
TBD To be determined
UT Unit Telescope
UTE Unit Telescope Enclosure
UTM Unit Telescope Mount

Table of Contents

1 Introduction

The FTT/NA system is one of a large number of opto-mechanical systems that comprise the Magdalena Ridge Observatory Interferometer. Although it is not the largest or most costly – these awards go to the delay-line system and the unit telescopes respectively – the role played by the FTT/NA system is a vital one. Before discussing how we envision that role might be satisfied, through an elaboration of the conceptual design for the FTT/NAS, we provide below brief reviews of two key areas of technical background that are pertinent to the remainder of this document. The first focuses on how the FTT/NAS fits into the overall architecture of the MROI, while the second reiterates some of the most critical high-level requirements that the top-level science goals for the MROI have placed on the system. We hope that these preliminary paragraphs will provide valuable context for the reader, and make clearer some of the design decisions we have taken over the past few months during our conceptual design activities.

1.1 MROI System Overview

As in most astronomical optical/IR interferometers, the light path from the location at which the radiation from a source is first intercepted by an individual unit telescope (UT) to the place at which it is eventually detected is a long and complicated one (see Figure 1). This path can be conveniently described as involving a sequence of legs along each of which a collimated beam of light is transported between a pair of opto-mechanical systems. Each of these systems is responsible for conditioning the optical beam in some way or another prior to the beam being sent onto the next system. At the MROI this sequence of steps can be summarized by the entries in Table 1.

As can be seen from Table 1, the FTT/NA system is the third opto-mechanical assembly that the light from a target will meet on its path to the beam combiners. As its name suggests, its primary roles are two-fold:

1. To acquire the target – sensing its location in a wide field of view image and using the position of the target relative to a pre-determined location in the sensor field of view to provide signals to be used to adjust the pointing of the telescope;

2. Thereafter, to detect and eliminate rapid tip-tilt (i.e. angle of arrival) fluctuations in the incoming light beam due to atmospheric perturbations – sensing these by, again, measuring the position of the target relative to a pre-determined location in the sensor field and using these measurements to send high-frequency control signals to the active secondary mirror of the telescope and low-frequency pointing corrections to the UT mount.

The location of the FTT/NA system, on the Nasmyth table attached to the eastern-most end of each UT, was frozen during the early stages of the architecture of the MRO interferometer and so has not been considered as one of the degrees of freedom associated with the conceptual design task described in this document. Similarly, the decision to use dichroic separation to split the "short" wavelength light needed by the FTT/NA system from those wavelengths to be sent to the interferometric instrumentation was frozen at the same time (in order to maximize the interferometric throughput) and so has not been further assessed here either.[1]

Although the idea of, and methods for, controlling fast tip-tilt perturbations in an astronomical telescope are straightforward in concept, there are a number of critical differences between single-telescope and interferometer-based implementations that are worth identifying here. These principally relate to MROI-specific design choices and so may not be obvious to all readers.

- Although the primary roles enumerated above mention a "pre-determined" location on the FTT/NAS sensor, they do not explain how this fiducial "zero-point" is chosen and the process by which it is defined.

[1] The MROI Project Office has decided that initially the FTT/NAS sensor will use a bandpass from 600 nm to 1000 nm, but that once an optical interferometric instrument has been installed (this is not expected until at least 2014, during Phase II of the project implementation) the bandpass from 350 nm to 600 nm must be available as a switchable alternative.

System	Component mirrors	System type (Pass-through or pickoff)	Input beam diameter (geometric)	Output beam diameter (geometric)	System primary role
Unit telescope	M1,M2,M3	Pass-through	1400 mm	95 mm	Collects light and compresses beam
Atmospheric dispersion corrector	n/a	Pass-through	95 mm	95 mm	Corrects for differential refraction between different colours
FTT/NAS	n/a	Pickoff	95 mm	95mm	Diverts short wavelengths towards the FTT/NAS sensor
Relay system	M4, M5	Pass-through	95 mm	95 mm	Relays longer wavelength beam towards optics laboratory
Delay line system	M6 (twice), M7	Pass-through	95 mm	95 mm	Adjusts optical path of light beam
Beam compressor	M8, M9	Pass-through	95 mm	13 mm	Compresses beam diameter
Beam turning mirror	M10	Pass-through	13 mm	13 mm	Diverts beam towards correlator tables
Science switchyard	Dichroic and 1 or 2 mirrors	Pickoff	13 mm	13 mm	Diverts shorter wavelengths towards science beam combiner
Fringe tracker switchyard	3 mirrors	Pickoff	13 mm	13 mm	Reflects remaining longer wavelengths towards fringe tracking beam combiner

Table 1: Summary of sequence of optical systems that the light from the target follows as it passes from the unit telescopes to the science and fringe-tracking beam combiners.

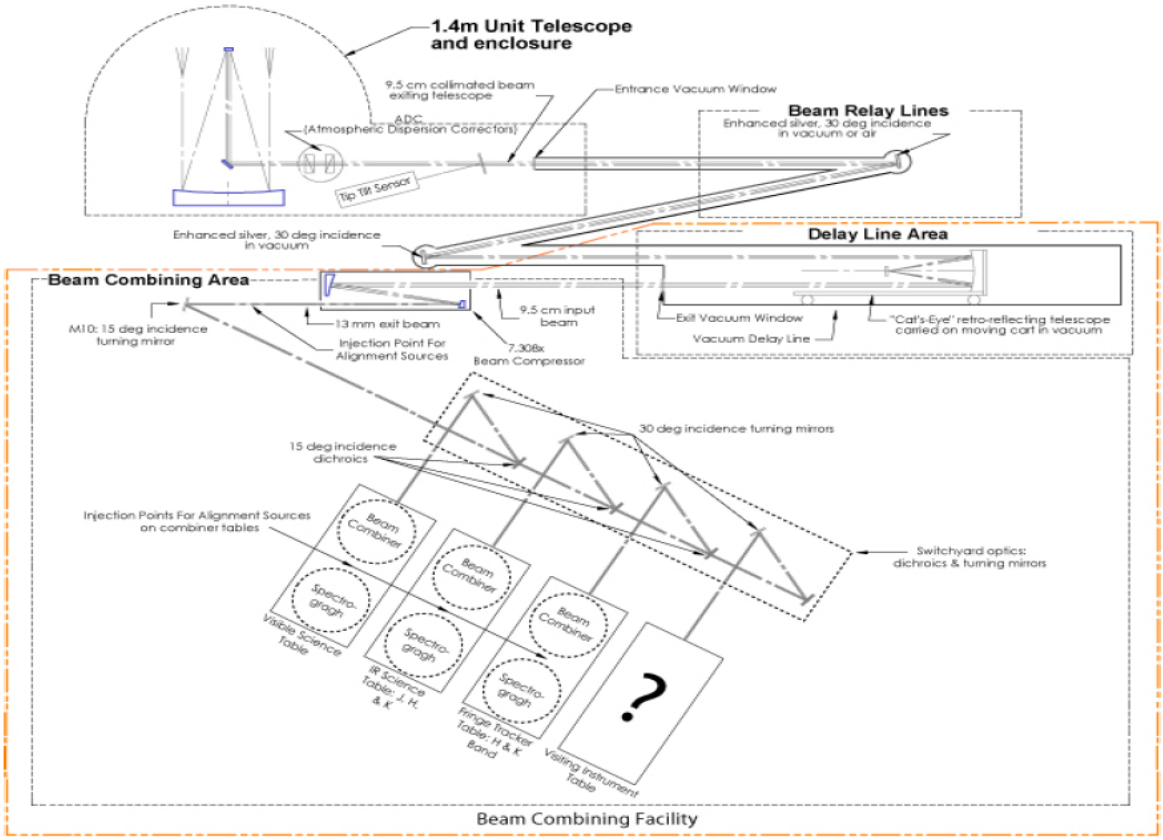

Figure 1: Illustration of the optical layout of the MROI showing the light-path from an individual UT (top left) to the beam combining instruments shown schematically at bottom left.

In fact, at the MROI this zero-point represents the guiding-centre (hereafter we shall refer to the guiding centre as the "objective-point") on the FTT/NAS sensor which will guarantee that the light being sent to the beam combining laboratory will be delivered to the interferometric instruments[2].

At the MROI, the location of the zero-point will be realised each night, prior to observing, by sending co-aligned and parallel light beams simultaneously to the interferometric instruments and to the UTs. The instruments in the beam combining laboratory will be aligned with respect to the inward-propagating beams, while at the UTs the outward propagating beams will be directed onto the FTT/NAS sensor after back-reflection from the FTT/NAS dichroic, retro-reflection off a corner-cube installed on the UT Nasmyth table and subsequent transmission through the FTT/NAS dichroic (see Figure 2 in Sec. 3).

Because it is a system goal to perform this registration of the zero-point only once per night, very stringent requirements have been placed on the stability of the optics through which the internal alignment beams are transmitted to each UT. Most of these optics will be located in the temperature controlled BCF, but two of them, the M4 and M5 mirrors, will be exposed to much larger temperature swings during the night (the median ΔT between sunset and the coolest time of the night at the MROI site is 5 °C). In the system error budget the total two-axis allocation for uncontrolled jitter and slow drift for each of M4 and M5 is 0.015 seconds of arc (referred to the sky). We note that this is the same allocation given to the stability of the FTT/NAS zero-point due to any instabilities in its optics and sensor, and indeed the same tilt stability requirement has been allocated to most of the other opto-mechanical systems enumerated in Table 1.1. We believe that this level of opto-mechanical stability is atypical for most FTT systems installed on single telescopes and much more stringent than is usual for those applications.

[2] More strictly, the zero point represents the objective-point for a target which is observed by the FTT/NA system and the interferometric instrument at the same wavelength, i.e. there is no differential atmospheric refraction between the guiding and science beams.

- An additional complication of the MROI FTT/NAS implementation is the fact that the light used for sensing the instantaneous position of the target image will be a different colour – in fact it will always be bluer – to that sent to the interferometric instruments. This is the reason that an Atmospheric Dispersion Corrector is the first system that light encounters after reflecting off the UT tertiary mirror (see Table 1). However, in its initial operational phase, the MROI Project Office has planned that an ADC will not be installed at each UT. As a result the objective-point on the FTT/NAS sensor will need to be deliberately offset from the zero-point established by the outgoing alignment beam from the interferometric laboratory to accommodate the difference in colour between the light being sent to the FTT/NAS sensor and to the interferometric instrument. This atmospheric dispersion offset will be pre-computed by the Interferometer Supervisory System (ISS) based on the colours and elevation of the target and the bandpasses being sent to the FTT/NAS and interferometric instrument. Updated values will be made available to the FTT/NAS at a rate of approximately 0.1 Hz by the ISS.

  In order to mitigate against uncertainties in the colours of the target source, the FTT/NAS is also required to permit small-angle synchronous dithering of the beam sent to the interferometric instruments so as to optimize the flux sent to them. Again, we believe this is a design feature not usually seen in single telescope FTT systems.

- Another feature of the FTT/NAS that relates to its role as a part of an interferometer (as opposed to any single telescope implementation) is the model that has been developed for its control. As for all the other interferometer systems, the operation of the FTT/NAS will be managed by the Interferometer Supervisory System. This will be responsible for sequencing all components of the array, for receiving and publishing (where necessary) all telemetry and status data sent by the systems, and for providing ancillary information, for example dispersion offsets, to the array systems. This framework, however, also assumes that the individual systems will be largely "self-sufficient" and it is required that each system can operate and monitor its own performance independently. This level of in-built intelligence may be unusual when compared with other FTT installations.

- One final, and perhaps unusual, feature of the FTT/NAS procurement is that the active optical component of the system, the UT secondary mirror, will be supplied independently by AMOS (the UT vendor) and its sub-contractor Physik Instrumente. The performance of this component, and the related requirements associated with the FTT/NAS, have been carefully specified so as to allow for predictable performance of the complete closed-loop fast tip-tilt system when all its components are eventually integrated at the Magdalena Ridge.

1.2 Top level requirements

The top level requirements associated with the FTT/NA system, and the less challenging requirements for the UT First Light Camera (FLC), are presented in detail in RD1 and AD2 respectively. The following brief list, however, summarises some of the most critical of the FTT/NAS requirements (RD1):

- Management of time varying offsets due to atmospheric dispersion and/or off-axis guiding;
- Supporting the streaming of "live" diagnostic telemetry;
- Supporting a synchronous dither of the output beam direction;
- Supporting both acquisition and fast-guiding modes;
- Realising the sensitivity desired for faint-source science;
- Realising the zero-point stability requirements, especially in an exposed variable-temperature environment;

- Meeting the thermal dissipation budget;
- Designing a system that is compatible with the space constraints present on the Nasmyth optical table.

This is neither an exclusive nor ranked list, but serves simply to highlight some of the most challenging issues we have had to address as part of our conceptual design activity.

1.3 Relationship between the FTT/NAS and the First Light Camera (FLC)

It may be helpful to review here the relationship between the FTT/NA system and the FLC since these two sequential deliverables will share certain hardware and software. Apart for the relatively straightforward difference associated with the timing of their delivery – the FLC will arrive at the MROI site roughly a year earlier than the complete FTT/NA system – the main distinction between these two systems will be their respective roles. The FLC is being designed primarily to facilitate acceptance testing, system integration, and evaluation of the UTs and the ISS, whereas the FTT/NAS will be responsible for providing the full functionality needed for acquisition and slow and fast guiding of the UTs during interferometric science observations.

The Cambridge group have been charged with the conceptual design of both systems, but the FLC conceptual design is the subject of a different document to this one. We refer to the reader to that document for further details of our proposed implementation for the FLC, but wish to make two brief comments here:

1. It is expected that it will be possible to run the FLC software with the FTT/NAS hardware when the FTT/NAS is eventually delivered;
2. It is expected that certain hardware elements will be identical for both the FLC and FTT/NAS implementations. The most obvious example of this is likely to be the sensor head for both systems, but, depending on progress on the detailed design work for the FTT/NAS, other hardware elements might be shared too.

2 Derived Requirements

This section summarises the "derived requirements" and error budgets which apply to particular components of the FTT/NAS. These have been calculated from the top-level requirements specified in RD1, on the basis of a minimal set of assumptions about the FTT/NAS conceptual design. Only the results of the calculations are presented in this document; descriptions of the methods and reasoning used are provided in RD2.

2.1 Assumptions

In order to quantify the derived requirements it has been necessary to make certain assumptions about the conceptual design of the FTT/NAS. The main assumptions, used to obtain the specifications listed in several of the subsequent sections, were as follows:

- We assumed that a single camera is used for target acquisition and fast tip-tilt sensing and that the same focusing optic(s) are used to image the target onto the camera in all operating modes;
- We assumed that the camera is an electron-multiplying CCD (EMCCD) with 512×512 pixels and a read noise of 50 electrons RMS.

Further assumptions are described in the subsections below to which they apply.

2.2 Pixel scale

The pixel scale for the FTT/NAS shall be between 0.12 and 0.2 arc seconds per pixel. The lower limit is set by the NAS FOV requirement, and the upper limit is based on an assessment of the centroiding accuracy needed in FTT mode.

2.3 FTT mode sub-frame size

To allow for field rotation over a 300 second observation when using an off-axis tip-tilt reference, the fast tip-tilt mode subframe dimensions must be at least $3.6'' \times 3.6''$. For the range of pixel scales above, this subframe size corresponds to between 18 and 30 pixels square.

2.4 Image quality

To allow for accurate centroiding under the best seeing conditions expected, we require the PSF width to be no greater than one detector pixel. Table 2 presents a summary of the maximum allowed displacements on each of the optical elements for our preferred optical layout (see Sec. 4.3) that leads to a 50% encircled energy diameter no greater than the width of one detector pixel. We have assumed observations of a target at the edge of a 10 second of arc field of view, corresponding to the use of an off-axis tip-tilt reference object. The values in the table were obtained by constructing a ZEMAX model of the layout and perturbing each element in one degree of freedom at a time until the 50% encircled energy diameter increased above one pixel i.e. 16 µm. An observing wavelength of 600 nm was assumed.

2.5 Stability of tip-tilt zero point

Table 3 shows the error budgets for the maximum allowable component displacements that meet the top-level zero-point stability budget for our preferred optical layout.

2.6 Thermal management

A number of derived requirements have been determined from the top-level heat dissipation requirements and the specifications of the candidate EMCCD cameras (Sec. 5.2.4), using the thermal modelling methods described in Sec. 7.1.1.

We have assumed that the EMCCD camera is placed inside an environmentally-controlled enclosure, in particular that:

- The camera enclosure temperature is controlled to protect the camera, to minimize heat dissipation to the environment when operating at night, and to ensure that the exterior surface temperature of the camera enclosure is within 2 °C of ambient;
- That the camera environment be controlled at all times, even though the camera may not be switched on (this ensures that the camera can be switched on without first having to warm up or dry the enclosure);
- Heat will be removed from the camera and the enclosure by fluid at a controlled temperature and flow rate and exchanged into one of the coolant loops available in the telescope enclosure.

Under these assumptions the derived requirements are as follows:

1. Maximum enclosure internal air temperature: 30 °C;

Element	Degree of freedom	Tolerance
Dichroic	δx	
“	δy	
“	δz	> 5 mm
“	$\delta\theta_x$	0.37°
“	$\delta\theta_y$	0.37°
“	$\delta\theta_z$	
Focusing lens	δx	> 5 mm
“	δy	> 5 mm
“	δz	0.35 mm
“	$\delta\theta_x$	0.93°
“	$\delta\theta_y$	0.93°
“	$\delta\theta_z$	
Fold mirror #1	δx	
“	δy	
“	δz	0.17 mm
“	$\delta\theta_x$	0.65°
“	$\delta\theta_y$	1.9°
“	$\delta\theta_z$	
Fold mirror #2	δx	
“	δy	
“	δz	0.22 mm
“	$\delta\theta_x$	0.77°
“	$\delta\theta_y$	1.2°
“	$\delta\theta_z$	
FTT/NAS sensor	δx	
“	δy	
“	δz	0.35 mm
“	$\delta\theta_x$	> 5°
“	$\delta\theta_y$	> 5°
“	$\delta\theta_z$	

Table 2: Individual element tolerance in position and angle that lead to a 50% encircled energy diameter of greater than one pixel (16 μm) for our preferred optical layout (see Sec 4.3). The focal length assumed was 1525 mm. For each element the z-coordinate represents the direction normal to the plane (or optical axis) of the component, while the x and y axes are orthogonal to this with the x direction perpendicular to the Nasmyth table.

Element	Degree of freedom	Budget allocation
Dichroic	δx	
“	δy	
“	δz	
“	$\delta\theta_x$	0.047″
“	$\delta\theta_y$	0.045″
“	$\delta\theta_z$	
Fold mirror #1	δx	
“	δy	
“	δz	0.59 µm
“	$\delta\theta_x$	0.090″
“	$\delta\theta_y$	0.049″
“	$\delta\theta_z$	
FTT/NAS sensor	δx	0.47 µm
“	δy	0.35 µm
“	δz	250 µm
“	$\delta\theta_x$	
“	$\delta\theta_y$	
“	$\delta\theta_z$	2.32″

Element	Degree of freedom	Budget allocation
Focusing lens	δx	0.47 µm
“	δy	0.35 µm
“	δz	250 µm
“	$\delta\theta_x$	0.75″
“	$\delta\theta_y$	0.70″
“	$\delta\theta_z$	n/a
Fold mirror #2	δx	
“	δy	
“	δz	0.31 µm
“	$\delta\theta_x$	0.064″
“	$\delta\theta_y$	0.074″
“	$\delta\theta_z$	

Table 3: Global error budget for the individual element tolerances in position and angle needed to meet the overall zero-point stability requirement for our preferred DLT layout (see Sec. 4.3). For each element the z-coordinate represents the direction normal to the plane (or optical axis) of the component, while the x and y axes are orthogonal to this with the x direction perpendicular to the Nasmyth table. The budget allocations are in all cases comparable to or larger than those for all the other layouts explored.

2. Minimum enclosure internal air temperature: 0 °C;
3. Minimum enclosure internal air/external surface temperature differential that must be accommodated: 3 °C (goal 8 °C);
4. Enclosure air dew point: coldest enclosure internal component -5 °C;
5. Enclosure residual heat 5 W;
6. Emissivity of outer surface of enclosure > 0.7;
7. Residual camera heat 20 W [TBC] (based on likely limitations of removing 15 W by unforced heat exchange with fluid);
8. Camera enclosure space envelope: arranged to fit potential layouts but expected to be 340 mm wide and 300 mm deep but no more than 350 mm high;
9. CPU and interface power dissipation allowance 180 W;
10. Camera interface and controller power dissipation allowance 70 W;
11. Power consumption allowance 350 W.

2.7 Closed loop bandwidth

We assume a frame rate of 1 kHz and a total compute latency of 100 microseconds. Hence a maximum readout latency (defined as the delay from the end of exposure to the pixel data being available for processing) of 1130 microseconds is needed to meet the requirement for 40 Hz closed-loop 3dB bandwidth. To meet the 50 Hz bandwidth goal, the maximum readout latency that can be tolerated is 790 microseconds.

2.8 Limiting Sensitivity

Table 4 gives the tip-tilt residual error budget for an observation of a m_v=16 active galactic nucleus (AGN), with the red colours defined in RD1, under the conditions specified in RD1. We have assumed a closed-loop bandwidth of 15 Hz, optimal for the specified seeing. The UT tilt residuals are from RD3 (but note that these values were specified at 10 Hz bandwidth – the true values for 15 Hz bandwidth could be up to 33% lower, i.e. better). The residual seeing tilt was calculated using the results from Tyler (1994).

Tilt error	**RMS error/ milliarcsec**	**Origin**
UT residual mount error	20	RD3
UT residual wind shake	30	RD3
Residual seeing tilt	30	Tyler (1994)
Speckle noise centroiding error	15	See text
Detection noise centroiding error	34	See text
Total	**60**	

Table 4: The two-axis tip-tilt error budget in seeing conditions of r_0=14 cm and turbulent layer wind speed V=10 m/s.

The speckle noise centroiding error is a bias that varies from frame to frame due to the centroiding algorithm not properly accounting for the multiple speckles making up each short exposure image. The magnitude of this effect will depend on the precise centroiding algorithm used, the choice of which will be investigated in the post-CoDR phase. For now we have adopted an intermediate value between that for conventional centre of mass algorithms and that for thresholded centre of mass algorithms.

We derive an allocation of 34 milliarcseconds for the two-axis "detection noise" centroiding error (the combined effects of photon shot noise and detector readout noise). Given realistic assumptions about the atmospheric, UT and camera window optical throughput and the CCD quantum efficiency, and assuming negligible read noise, we require the other FTT optics (dichroic, focusing optic, fold mirrors) to have 102% throughput. Hence the limiting sensitivity requirement cannot quite be met.

If we conservatively assume 85% throughput for these FTT optics, the total residual tilt is only some 2% over budget. This would result in an additional visibility loss in the H-band of merely 0.5% over what has been budgeted.

The detector read noise will have negligible performance impact (1% degradation of the centroiding accuracy) if the effective read noise is below 0.20 electrons per pixel, assuming a 6×6 pixel quad cell. This implies electron multiplication gains of at least 250 for an EMCCD with an output read noise of 50 electrons.

2.9 Dynamic range

We assume that the FTT mode frame rate will be 1kHz except for the very faintest stars. It is assumed that in the NAS mode the exposure time can be adjusted independently of the frame rate and that the minimum exposure time is 1 millisecond.

Under these assumptions, just two EMCCD amplification settings – corresponding to the use of no gain and a sufficiently high gain to reach the limiting sensitivity – can be used to allow observations spanning the magnitude range from 3.3 to 16 (in good seeing), for both FTT and NAS modes. Stars as bright as magnitude 1.8 could be observed in poor seeing. There is a 2-magnitude overlap between the faintest objects observable without amplification and the brightest objects observable with amplification, hence it should usually be possible to observe a science target and calibrator with the same gain setting. These magnitudes correspond to the red target colours specified in RD1, which are appropriate for AGN and red supergiant stars.

Observations of brighter targets will require the use of a pupil mask or neutral density filter to prevent the camera from saturating.

3 FTT/NA System Design

In this section we present a high-level overview of the proposed FTT/NA system conceptual design and outline the reasoning that has led us to select this system architecture. Our system concept is based around a commercial off-the-shelf back-illuminated EMCCD camera. This type of camera offers a combination of fast readout, high quantum efficiency and sub-electron effective read noise, which is needed to meet the stringent closed-loop bandwidth and limiting magnitude requirements of the FTT/NAS.

Our design is predicated on the same EMCCD camera being used for target acquisition and fast tip-tilt correction, with a fixed pixel scale. This implies a sufficiently large-format camera to satisfy the 60×60 arc second field-of-view requirement (or goal of 100×100 arc seconds). A minimum of 2.5 pixels across the short-exposure image FWHM was considered necessary for accurate centroiding (RD2), this pixel scale constraint leading to a minimum CCD format of 500×500 pixels. Larger-format cameras would have made it easier to meet the FOV goal, but were not considered for cost reasons and because they are slower to read out.

EMCCD camera manufacturers all specify that their cameras must be operated at a temperature above 0 °C, in a non-condensing environment, and so the FTT/NAS camera must be enclosed and a thermal control system be supplied to maintain the temperature and humidity inside the camera enclosure at all times. This system must

extract heat from the enclosure and dump it to a chilled fluid loop in order to prevent the camera overheating and to minimise heat dissipation to the air.

Figure 2: Block diagram of the FTT/NA system. In our system design, the "detector" is a COTS EMCCD camera, and additional fold mirrors may be used to redirect the light beam reflected from the dichroic and hence accommodate other systems installed on the Nasmyth optical table (see Sec. 4.1).

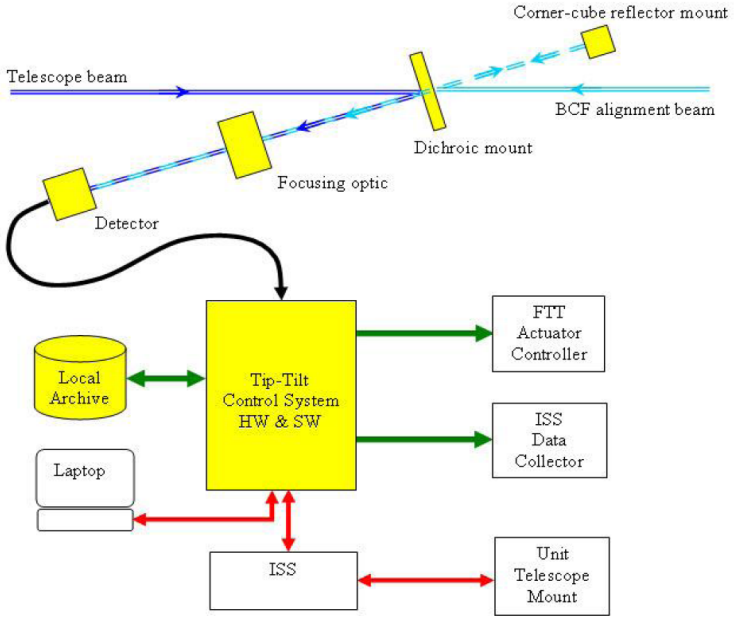

The FTT optics (shown conceptually in Figure 2, see also Figure 3 for specific candidate layouts) arranged on the Nasmyth table, together with the dichroic and the EMCCD camera, must remain sufficiently stable in tilt and displacement such that the tip-tilt zero point does not move by more than 0.5 μm on the detector surface over a night's observations. To meet such high stability requirements we have chosen to use mounts without adjusters for the optical components: every component, once aligned, will be fixed in position. This in turn will require the system to be tolerant of focus changes so that focus adjustment is only required seasonally. The stability requirements demand low sensitivity to thermal changes and so thermal gradients across component mounts must be minimised. This has led us to adopt aluminium rather than stainless steel or invar (which is too expensive) for the mount material.

A camera frame rate of 1 kHz and a latency < 790 μs are needed to meet the goal of a 50 Hz closed-loop bandwidth for fast tip-tilt mode (RD2). We have established through our camera evaluation process that the preferred candidate camera can satisfy these derived requirements with a custom CCD clocking scheme. However, discussion with the vendor has indicated that a probable maximum subframe size of 23 × 23 pixels will likely be imposed by the CCD readout architecture. Provided the pixel scale is coarser than 0.15 arcsec/pixel, this subframe size will be sufficient, under worst-case conditions, to allow tip-tilt correction using an off-axis reference star for at least 300 seconds, before a brief (< 1 second) interruption to fast tip-tilt mode is needed to reposition the subframe. No such interruptions are anticipated for the more common case of on-axis guiding, or when the field-rotation for an off-axis guide star is smaller.

Although the FTT/NAS latency goal is demanding, we have chosen to close the fast tip-tilt loop in software rather than consider reconfigurable electronics such as FPGAs. We are confident that Xenomai real-time Linux, in conjunction with a real-time driver for our preferred camera, will allow the latency goal to be met comfortably, and that there will be sufficient CPU time for the data processing to derive the tip-tilt correction and for communication with the ISS using the MRO-provided interface software. This approach minimises the system's electrical power consumption, since only a conventional rack-mount PC is needed to satisfy all the computing needs (including thermal management of the camera enclosure). Basing our system on a standard

PC also allows us to make the most extensive possible use of software libraries provided by the camera vendor.

A fixed frame rate of 1 kHz will be used for all but the faintest targets (there is no noise penalty for this due to the on-chip amplification) but the closed-loop bandwidth will be user-selectable by means of adjustable servo parameters that allow the degree of time-averaging of the correction signal to be altered by the user/ISS.

A range of V-band magnitudes from 3.3 to 16 for the tip-tilt reference object can be accommodated simply by switching between a high EMCCD gain setting (~250) and zero gain at an appropriate magnitude (~8.5). If brighter objects are required to be observed, a means of attenuating the signal (such as a pupil mask or neutral density filter) will need to be introduced. Currently we have not yet included this feature in our conceptual optical design.

4 Optical Layouts

We have investigated a number of different optical layouts for the FTT/NA system. The following sub-sections describe various aspects of this task, including a review of the principal opto-mechanical constraints on any potential layout, the range of candidate layouts, the selection of a preferred layout and the reasons we believe this is the lowest risk route to follow.

4.1 Layout constraints

As may have become clear already from Sec. 2, some of the properties of the opto-mechanical elements of the FTT/NAS, e.g. the focal length of the focusing optics, are bounded because of their impact on meeting certain performance requirements. However, there are a number of other more practical boundary conditions which have constrained the range of optical layouts that we have been able to explore. These are enumerated below.

1. The finite size and orientation of the UT Nasmyth table, in particular its shorter dimension which runs parallel to the direction of the exit beam from the telescope tertiary mirror, has meant that all of the layouts we have considered have had to use fold mirrors;

2. The presence of additional systems on the Nasmyth table, a number of which are not moveable, has further constrained the range of feasible layouts. These are shown schematically in Figure 3 as the numbered boxes. Items 8 and 6 & 7 correspond to the future unit telescope ADC and adaptive optics systems respectively, and have been assumed to be fixed. Items 2 & 3 and 4 & 5 correspond to elements of the Automated Alignment System (AAS). While these must remain associated in pairs aligned with respect to each other as shown, each pair can be installed with some variation in its horizontal and vertical origin in the figure. This explains why the locations of items 2 & 3 are not identical in each of the candidate layouts.

   Two additional fixed components on the table are the M4 mirror unit and the corner cube component of the AAS. The corner cube appears towards the bottom left in all the panels of Figure 3 and is required to intercept the blue-coloured beam of light shown in the panels and send it back through the dichroic toward the FTT/NAS sensor. There is very little scope for locating this component anywhere else on the optical table. Similarly, there is no flexibility on the location of the M4 mirror unit because it has to divert the outward-going beam towards a fixed aperture in the enclosure wall;

3. As well as the components of other systems present on the Nasmyth table, the UT and its enclosure also severely limit the space envelope available for the FTT/NA system. In particular, there is a hard limit to the maximum height that any element of the FTT/NAS may present above the table surface. This has had most impact on the possible locations for the sensor head, and how it can be packaged in its thermal enclosure;

4. A final design degree of freedom that we have not been permitted to explore is the angular orientation of the dichroic mirror that serves to divert the bluer light to the FTT/NAS and transmit the interferometric beam. The interferometer system design has as a priority a requirement to allow the array to observe polarised targets in total intensity, and so the global optical layout of the array and the optical coatings have all been designed for angles of incidence of either 0° or 15°. The impact of this for the FTT/NAS is that the angle between the beam hitting the dichroic mirror and that reflected towards the FTT/NAS sensor has had to be fixed at 30 degrees.

A rather different issue that we have had to deal with is the extent to which any initial layout for the FTT/NA system must support future expansion of the capabilities of the MROI. This has been accommodated in two ways. First, all the optical layouts considered have not been allowed to encroach on the footprints of the AO and ADC systems (items 6 & 7 and 8 in the panels of Figure 3), even though these are not expected to be present for several years after first fringes have been detected. Second, all our layouts have left space surrounding the dichroic mount to allow a larger mount handling two switchable components to be installed when an optical interferometric instrument is installed. The design of such a mount is beyond the scope of this conceptual design, but we believe that we have been generous with our space allocation to allow this enhancement in Phase II of the MROI deployment.

4.2 Candidate layouts

The four main optical layouts we have considered are illustrated in Figure 3. We have studied both mirror and lens-based configurations, and describe the principal rationales behind each class of layout below. The astute reader may however already have noted two common features of all four of our generic layouts:

1. All the layouts have the dichroic mounted so as to send its reflected beam in the opposite direction to that of the exiting science beam. We were unable to find any layouts that used the complementary orientation without interfering with the elements of the AAS identified as items 4 & 5;

2. All the layouts presented exploit the use of a single baseplate upon which the dichroic mirror, the focusing optics, and any fold mirrors needed to feed the FTT/NAS sensor are co-mounted. The rationale for this is that this will mitigate, to first order, any local differential tilts or deformations in the Nasmyth table induced during the night due to changes in temperature. Such local disturbances would lead to differential movements and angular shifts of the FTT/NAS optical components and likely make the $0.015''$ zero-point stability requirement unrealisable.

Further commentary on each layout is presented below.

4.2.1 OAP layout

The Off Axis Parabola layout is conceptually a simple one. The beam diverted by the dichroic is intercepted by an off axis parabola, and focused onto the FTT/NAS sensor using a single fold mirror. It was not possible to find a layout that allowed the use of a sufficiently long focal length without folding the optical path, even using a custom parabola. A solution that had been previously considered, in which the sensor was held in an elevated position above the optical table surface, had to be discarded because it conflicted with the height of the space envelope available for the system. One noticeable feature of the OAP layout is the wide separation between the key optical elements, necessitating a rather long baseplate, and locating the sensor some distance away from the dichroic.

Figure 3: Illustrations showing the schematic arrangements of the four possible optical layouts for the FTT/NAS that have been considered. Clockwise from top left these are the OAP, DT, DLT, and Zoom configurations. In these layouts, which correspond to a UT located on western arm of the array, the beam transmitted to the beam combining laboratory enters the vacuum beam relay system at bottom left after being reflected off the M4 unit located to the left of each panel.

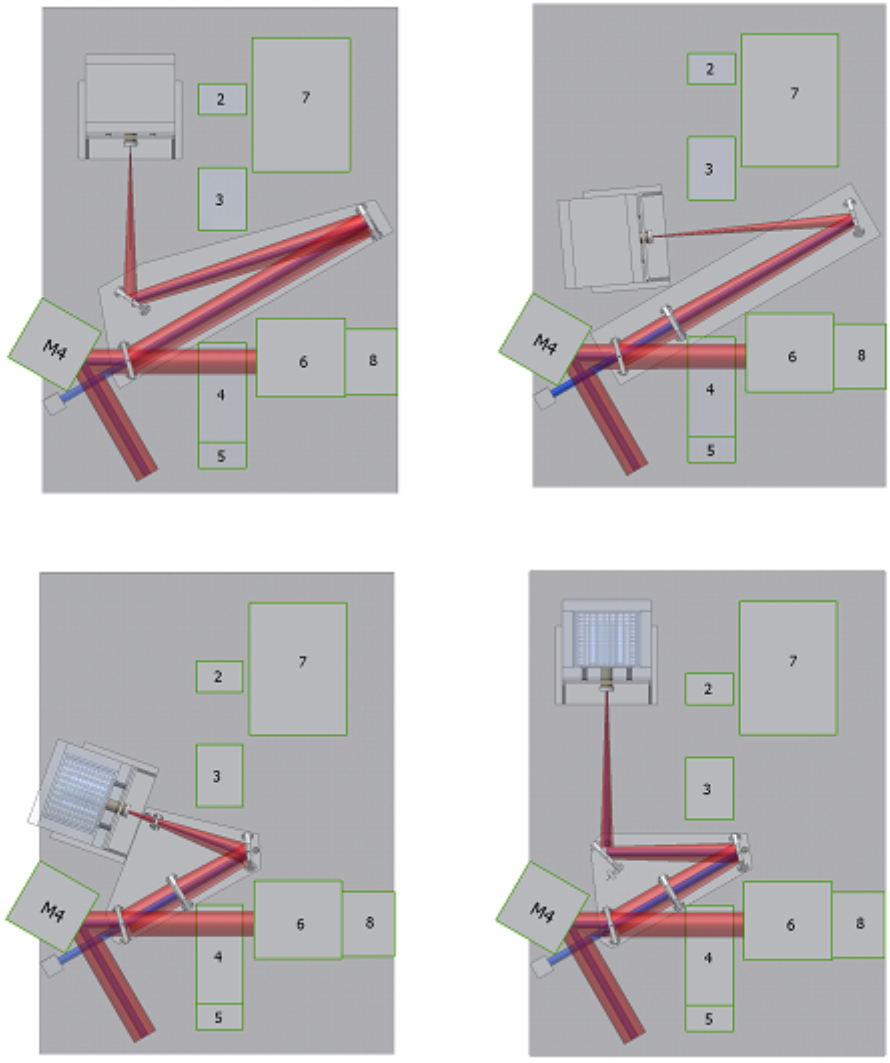

4.2.2 DT layout

The Direct Transmissive layout is the direct analogue of the OAP layout but using a lens rather than a mirror to effect the focusing of the beam. As for the OAP layout we were unable to find a layout that did not involve the use of a fold mirror. In this case however, it was possible to arrange the optical system to allow for the FTT/NAS sensor to be close to the other optical components, thereby reducing the possible variations in ambient conditions experienced by these elements of the system. The use of a lens, as opposed to an off-axis parabola, has the advantage that its field of view is larger – which leads to a beneficial reduction in the angular installation tolerances of the focusing optic by a factor of approximately 10 – and that uncontrolled tilting of the lens gives rise to much smaller focal plane shifts (by a factor of roughly 20) that the equivalent reflecting optic. Like the OAP layout, the DL layout has a need for a rather long baseplate to support its critical optical elements.

4.2.3 DLT layout

An interesting variation of the DT layout is its folded counterpart, which we have designated the "dog-leg transmissive" layout. This is very similar to the DT layout optically, but allows for a much more compact baseplate on which all four optical elements can be mounted. This helps mitigate against differential movements of the dichroic, lens, and two fold mirrors but this benefit is tempered by the fact that a long effective focal length can then only be accommodated by locating the FTT/NAS sensor some distance away. Furthermore, the use of an additional fold mirror delivers a slightly lower throughput and adds one extra element that needs to be mounted and installed.

4.2.4 Zoom layout

The final class of layout we have explored is one where the long focal length required to meet the top-level requirements is achieved through the use of a short focal length objective coupled with a much smaller negative lens placed close to the sensor focal plane. This is a "Barlow" configuration and allows for a very compact configuration for the FTT/NA system if a fold mirror is used between the two lens elements. In this case, not only is it possible to mount all the optical components on a small baseplate (comparable in size to that used in the DLT layout) but the shortening of the physical distance between the objective and the focal plane means that the FTT/NAS sensor can itself be butted-up alongside the plate. In addition, small movements of the second lens can be used to focus the system through moving a relatively small optical element.

4.3 Preferred layout

Once we had established that there existed layouts of the four architectures described above that would satisfy the opto-mechanical constraints outlined in Sec. 4.1, and which would be consistent with the optical flow-down from the top-level system requirements, the pros and cons of each layout were assessed and compared. The most important metrics used to assess the relative merits of each configuration were primarily mechanical and related to the sensitivity of a given layout to:

1. Component installation inaccuracies;
2. Temperature-induced misalignment during a night;
3. External mechanical perturbations.

A detailed opto-mechanical error budget for the mounting tolerances required for the four layout geometries can be found in RD2. We have not repeated that information here, but have provided some textual commentary of its implications in the discussion of each of the layouts below.

While the OAP layout has the merit of being an achromatic solution that can utilise a COTS optic, we were unable to find any implementation that did not require a long baseplate and that did not locate the dichroic, sensor and focusing optic at widely separate locations on the Nasmyth table. Alone amongst all the layouts, the OAP configuration requires its focusing optic to be stable in angular orientation on the table to roughly 1/20$^{\text{th}}$ of a second of arc. This is twenty times the requirement for the lens-based layouts, where stability at the level of 0.7 seconds of arc will suffice. In addition, the initial installation tolerance for the parabolic optic is roughly 3 minutes of arc, a factor of nine tighter than the single-lens solutions. Perhaps most importantly though, the OAP is located close to one edge of the optical table, and the resulting need for a rather long baseplate implies a much poorer lowest resonant frequency for the baseplate than the more compact plates used in the DLT and Zoom configurations (45 Hz vs 110–140 Hz, see Sec. 6.2.1).

The DT layout improves on the OAP configuration by using a focusing optic that is much more tolerant of initial angular installation errors and subsequent angular drifts, is more straightforward to mount, and allows for the FTT/NAS sensor to be located much closer to the centre of the Nasmyth optical table. Our optical analyses with ZEMAX have indicated that a custom apochromatic optic will be required, but we have already identified a preliminary design that meets the optical quality requirements for all bandpasses and temperatures required and utilises glasses that are readily available (see Figure 4).

Figure 4: Polychromatic spot diagrams for a 1.5 m focal length cemented achromatic triplet comprising SSK8, KZFS4 and BALF5 elements. The blue, green and red symbols code for observing wavelengths of 400 nm, 600 nm, and 900 nm respectively. The spot diagrams are overlaid on a 5 µm pixel grid, so that the total extent of each panel is 5 µm × 5 µm. In all cases the 50% encircled energy diameter is less than 16 µm. The sequence from left to right corresponds to the ambient temperature changing from -5 °C to +10 °C in 5 °C intervals. An expansion coefficient for the optical table surface of 17 µm/m/K has been assumed.

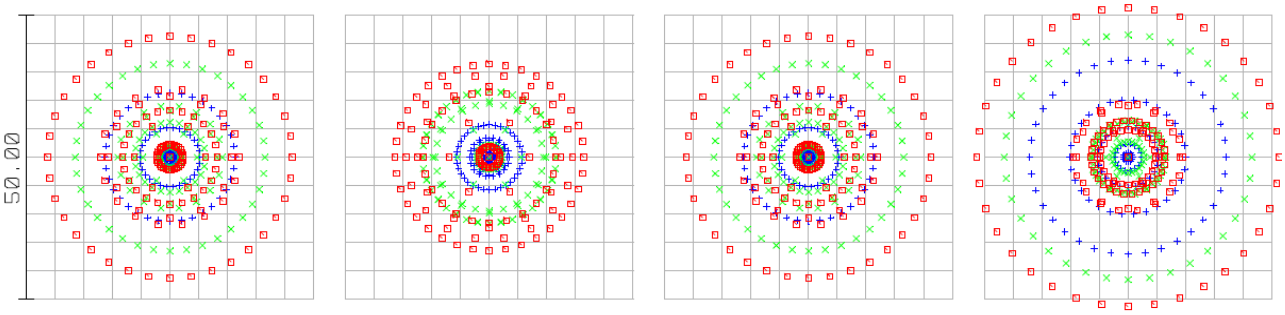

The major shortcoming of the DT layout is that it requires a slightly less stiff baseplate than the OAP configuration, with a lowest eigenfrequency of only 37 Hz. All the layouts considered require that the FTT/NAS dichroic be stable in angle at the ~0.05″ level to satisfy the overall error budget for the night time zero-point stability, and so this low eigenfrequency and the large physical extent of the DT baseplate render this layout less than optimal.

The most attractive layout we have found is the DLT configuration. This combines the benefits of a lens-based design with a very compact baseplate such that all four of the key optical components of the FTT/NA system are in close proximity. Perhaps its only shortcoming is that the FTT/NAS sensor is required to be located far from these optical elements because of the long focal length required.

The final layout investigated – the Zoom layout – offered the prospect of combining a compact footprint for the main optical components of the system with a physically small space envelope for the overall system (including the sensor). In particular, we had hoped to capitalise on the ability to butt the sensor mount up against the optical baseplate. However, we have been unable to date to design an apochromatic pair of lenses that can deliver the image quality the system needs for the two desired bandpasses at any temperature, let alone for the range of temperatures needed. The speed of the larger first lens appears to be the problem, and so on these grounds we have had to rank this layout as poorer than the DLT layout at this moment in time.

We have therefore selected the DLT layout as the most promising to adopt on the basis of its compact footprint, the feasibility of realising a suitable focusing optic, and because the allocations in its opto-mechanical stability error budget are in all cases no worse than any of the other competing layouts. However, we intend to continue to investigate the design of suitable optics for the zoom layout in the near term, since if these can be realised effectively, then the most compact layout may become available.

In our previous Table 3 we have shown the components of the opto-mechanical error budget for the DLT layout to remind the reader of the rather challenging demands that the night time zero-point stability requirement implies. Further sections of this document will present our analyses showing why we believe this error budget is attainable.

4.3.1 Variations

At the present time we have yet to fully explore a number of possible variations on the DLT layout. Notably, we have not attempted to optimize the layouts for the size and/or shape of the baseplate, nor have we assessed how allowed changes in the focal length of the focusing lens may impact the mechanical stability of the system and the optical performance achievable with the lens. Furthermore, we have not yet completed our optical design search for achromatic lenses suitable for the Zoom layout. We expect to explore these as our design work continues.

4.3.2 Feasibility

Our initial analyses suggest that the conceptual optical design we have selected appears to be the most promising to follow. The opto-mechanical stability required is challenging, but no worse than any of the other layouts we have explored. Our optical analysis suggests that a custom triplet lens design will likely be required, but we are very confident that a satisfactory cemented design will be feasible at a price comparable with that of a custom off-axis parabola.

The use of a lens-based solution at first sight appears to be potentially more lossy than a reflective solution, but COTS anti-reflection coatings can have losses averaging less than 1% across the bandpasses of interest to the system (see, e.g. Figure 5), and we have already have ROM costs for custom coatings a factor of two better than this. These surface losses are smaller than those expected at, e.g., an overcoated silver mirror, and so when combined with a cemented lens design, we expect comparable throughputs for both lens-based and reflective optical architectures.

A final critical aspect of performance is the need to procure a suitable dichroic. This is a key element of the FFT/NAS regardless of which layout is eventually adopted. We already have designs for both the Phase I and Phase II dichroics (see, e.g., Figure 6) and it only remains for us to optimize these for the specific material properties used by our selected vendor before we can have these fabricated.

5 Camera selection

Given the stringent top level requirements for the FTT/NA system in the areas of closed-loop bandwidth and optical sensitivity, the search for a suitable sensor head was a one of the highest priority tasks at the start of our conceptual design studies. Not only were latency and broad-band optical efficiency important, but the ability to run the sensor head in the hard real-time mode needed for closed-loop operation featured very high in our decision matrix. In the following sub-sections we review the results of our investigations.

5.1 Candidate cameras

As part of our design task we surveyed the market for cameras with the following attributes:

Figure 5: The typical performance of a COTS broad-band anti-reflection coating, in this case for a Melles Griot HEBBAR design, across the bandpasses required for the FTT/NA system. Custom coating designs can realise losses as low as 0.5% across the same bandpasses if required.

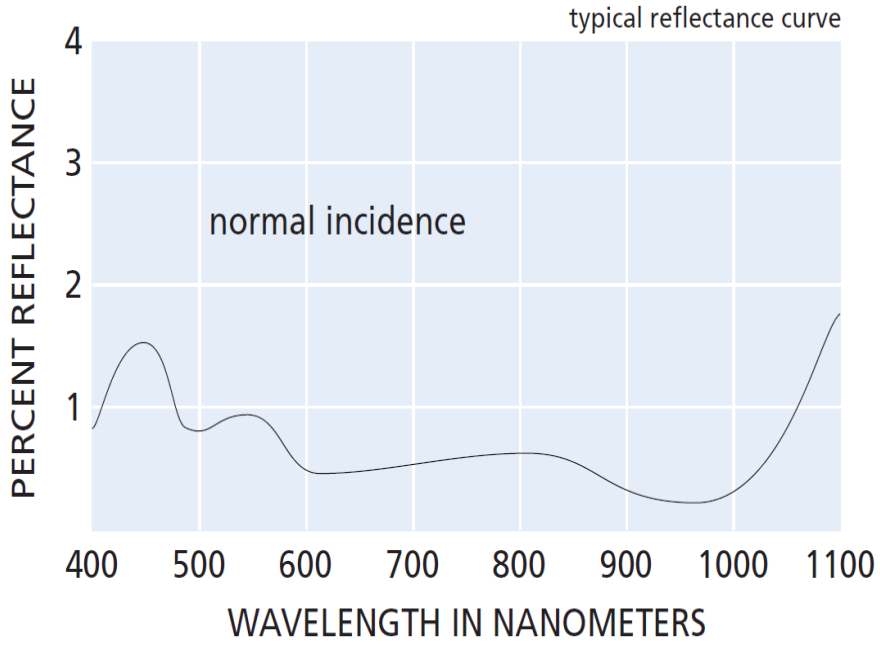

Figure 6: Predicted dichroic performance for the current design of the Phase I FTT/NAS dichroic. The red and blue curves refer to the two orthogonal linear polarization states. Between 600 nm and 950 nm the mean reflectance is greater than 99%, while within the J, H and K near-infrared windows the transmission is greater than 99%. Experience with a previous, albeit less optimized design (mean reflectance ≈ 96%), showed agreement between the measured and design performance at better than the 1% level over the full 600 nm to 2400 nm passband).

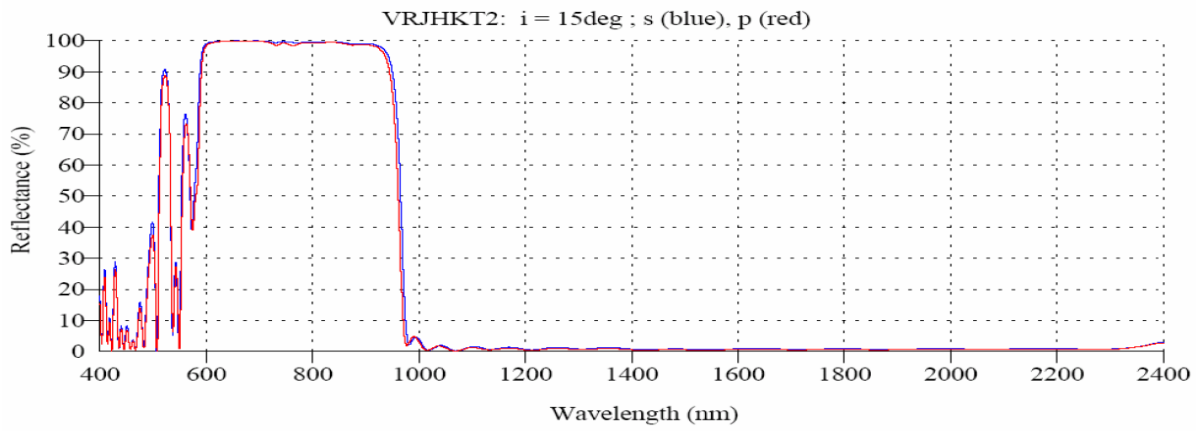

1. Use of a back-illuminated EMCCD detector. This is the only commonly available detector with the sensitivity, readout rate and noise characteristics needed to meet the fast tip-tilt system requirements;
2. Presence of a detector array size of at least 500 × 500 pixels, to permit narrow-field acquisition as well as fast wavefront sensing;
3. Capability for rapid readout, digitisation, and fast transfer of data to a host computer, to maximise the bandwidth of the fast tip-tilt servo loop;
4. Availability of a water cooling option. Fan-forced air cooling contributes to vibration and local air turbulence and so was deemed unsuitable for our application;
5. A significant vendor presence both in the United Kingdom and the United States, to ensure straightforward procurement and support in both places.

Based on these criteria, two cameras that were well known within the physics community were chosen for laboratory testing: the Andor iXon^{EM}+ 897 and the Princeton Instruments ProEM 512B. A third camera, the Hamamatsu ImagEM C9100-13, was identified as a possible reserve candidate and examined only through documentation and vendor enquiries.

5.2 Camera evaluation

Our evaluation was broken down into an assessment of the following major topics:

- Pricing
- Hardware considerations
- CCD clocking
- Power, environment and cooling
- Latency and programming considerations

The findings from each category are tabulated below alongside a discussion of the major points.

5.2.1 Pricing

The prices of the cameras are shown in Table 5. On the basis of price, the ImagEM C9100-13 was favoured, though in reality the price differential between all the systems was relatively small.

Attribute	Requirement	iXon+897	ProEM 512B	ImagEM C9100-13
Approximate price/GBP		25k	25k	18k

Table 5: Prices of candidate EMCCD camera systems.

Attribute	Requirement	iXon+897	ProEM 512B	ImagEM C9100-13
Sensor		e2v CCD97	e2v CCD97	e2v CCD97
Maximum data cable length/m	>TBD (goal >5.5)	6	50	10
Peripherals		Peltier cooling supply, cable length not measured	Camera power supply, 3m cable	Camera controller (big), cable length 3, 5 or 10m
Computer interface		PCI	Gigabit ethernet	Camera Link
Mounting		Screws into CCD frame side or front	Screws into CCD frame side	Mounting bracket underneath
Case		Plastic/polymer Awkward shape	Metal, rectangular	Looks metal, rectangular
Mechanical CCD stability		Stable	Stable	Untested

Table 6: Summary of hardware considerations for camera evaluation.

5.2.2 Hardware considerations

The hardware attributes we considered are summarized in Table 6.

All three cameras use the same physical sensor: a CCD97 back-illuminated electron multiplying CCD sensor manufactured by e2v technologies. This is a 512 × 512 pixel frame-transfer device with 16 µm × 16 µm square pixels and a quantum efficiency that peaks at 93% at 575nm wavelength.

The iXon^{EM}+897 head derives both power and data services from a cable connected to a custom PCI card in the host computer. A separate laptop-style DC power supply powers the head's Peltier cooler. The 6m maximum data cable length for the Andor head is a hindrance because the cable run between the Nasmyth table and the rack allocated to the host computer is already close to 5.3 m long. This may mean that the possible location of the camera is restricted. However, we have already identified an alternative cable routing with the help of the MROI Program Office, and so if a shorter alternative routing is needed we believe one is available. The Andor camera case, while compact, is an awkward shape and does not sit flat on an optical table, it must be raised or suspended. However, we have established that it is possible to do so without compromising its stability.

The ProEM 512B has a rectangular case that can be straightforwardly and stably mounted. It connects with its host computer via gigabit ethernet, with all the networking flexibility that ethernet brings. Most relevantly, it can be mounted up to 50m away from its host computer. A separate power supply powers both the Peltier cooler and the camera electronics through a single cable.

The ImagEM C9100-13 camera head is also contained within a easily mounted rectangular case. A separate controller box provides power and some data services to the head. The camera uses a Camera Link cable to communicate with a Camera Link card within the host computer. The controller box would occupy an area about the size of an A4 sheet of paper in the control rack, which would reduce the space available for other equipment but could be accommodated.

As part of our assessment, lab tests to determine how each candidate camera's CCD moved when the camera was stressed by temperature changes were undertaken. This was because our optical tolerancing had already indicated that an unanticipated lateral CCD movement of more than half a micron during a night's observing (Table 3) would cause an intolerable perturbation in the zero-point position. Stability of the CCD was tested in-house because none of the vendors specify it.

Our test involved imaging a distant point light source onto the CCD via an independently mounted lens (Figure 7). The image provided a submicron-stable, contactless reference position on the CCD. Using the vendor-

supplied demonstration software, the operational temperature of the CCD was changed and a series of images were captured at 1 Hz over periods of 10 to 20 minutes and written to file. The centroids of the light source position within each recorded image were then extracted with subpixel accuracy. If the CCD moved, the position of the centroid would shift relative to the CCD pixels.

Figure 7: Method for determining mechanical stability of a CCD with respect to the vendor's housing.

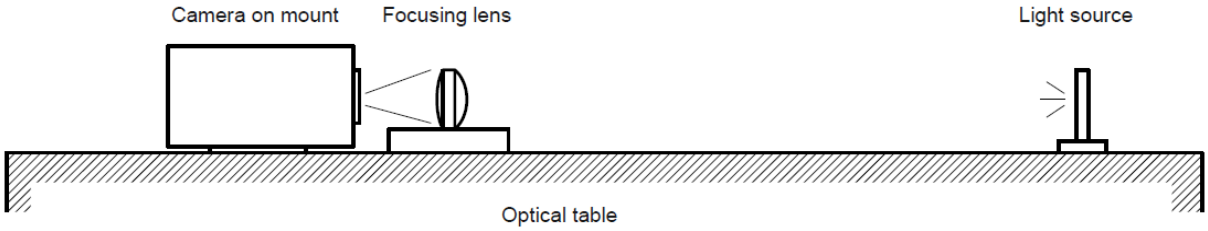

The ProEM 512B CCD was found to be stable to within 0.5 microns (horizontal) and 1 micron (vertical) for CCD temperatures in the range +20 °C to -70 °C. However, the iXon^{EM}+897 CCD was found to change height by up to 8 microns as the CCD temperature ranged from +20 °C to -85 °C. Upon investigation it was found that a change to the set temperature also changed the temperature of the air blown out of the camera ventilation grills (the Peltier power had changed), which in turn changed the temperature of the aluminium mount supporting the camera. After the test was refined to include temperature and expansion measurements of the mount, it was found that the height changes could be accounted for entirely by thermal expansion and contraction of the mount. No such problem was encountered with the ProEM 512B since it was much more simply mounted from underneath, away from its air vents. The ImagEM C9100-13 was not tested.

After correcting for mount expansion, the iXon^{EM}+897 CCD was found to be stable to within 1 micron relative to the camera housing.

It should be noted that this movement occurred over a large temperature change of the chip and its Peltier interface. There was no evidence that there is movement of the chip once cooled to its operating temperature.

On-site, the fast tip-tilt camera will operate at a fixed CCD temperature and be housed in a box where the air temperature will only change by at most 2 °C during a night. Hence the risk that either candidate's CCD will move beyond the required tolerance is low. Neither camera is preferred over the other based on this criterion.

5.2.3 CCD clocking

The clocking and readout capabilities of the candidate cameras are summarized in Table 7.

Cameras with faster readouts are to be preferred, because this will improve the fast tip-tilt servo closed-loop bandwidth. However, on the basis of the performance data tabulated above no camera stands out. The ImagEM C9100-13 has the fastest serial clock, but also a slower full frame-rate than the others, which implies an unspecified delay somewhere else in the signal chain. The iXon^{EM}+897 is slightly, but not significantly, preferred.

All three manufacturers specify dark current, readout noise and clock induced charge noise figures for their cameras. Dark current is not expected to be an issue for the FTT/NAS because the camera will be cooled and the exposure time will always be short. The readout noise will be more important because it will determine how much electron multiplying gain will is needed to overcome it, and this has implications for the available dynamic range. Clock induced charge is an artefact of the rapid readout and can be problematic if not controlled.

These vendor-supplied noise specifications do not significantly discriminate between cameras. Although the Hamamatsu has an edge in terms of readout noise, all cameras are likely to be equally capable of delivering an adequately low noise level.

Finally, audio transduction was noticed in the ProEM 512B device. The readout was audible as a faint buzzing sound, while gently tapping the head caused light streaks to appear in images.

Attribute	Requirement	iXon+897	ProEM 512B	ImagEM C9100-13
Shortest parallel clock time/ns		300	450	Not specified
Shortest serial clock time/ns		100	100	91
Max full frame rate/ Hz		35	34	31.9
Dark current/ (e-/pixel/s)		0.001 at -85 °C	0.001 typ, 0.02 max at -70 °C	0.001 at -80 °C
Clock induced charge/(e-/pixel/s) at 1000× gain, 30 ms exposure		0.01	0.01	0.01 (1200 × gain)
Readout noise/e- at 10 MHz		49	50	25 (11 MHz)
Readout is audible at head		No	Yes	untested
Head microphonics		Not noticed	Yes	untested

Table 7: Summary of the readout performance of the candidate EMCCD cameras.

5.2.4 Power, environment and cooling

The measured and manufacturer power dissipation data are presented in Table 8.

Power dissipation in the camera head is an important consideration for thermal management of the FTT/NAS, because excess camera heat must be removed from the Nasmyth table without perturbing the local air. In the candidate cameras, the heat from the Peltier cooler is easily removed via the water cooling system provided, but residual heat is also generated by the other camera components and this needed to be quantified before a thermal management solution could be proposed.

The actual power dissipation was determined in two ways. Firstly, the current and voltage feeding the camera head were determined, either by direct measurement or through a vendor enquiry, and broken down into Peltier and non-Peltier components. The power was calculated from these values. Secondly, the rise in temperature of fan-forced air through the camera was measured with the Peltier cooler either off or on, and together with an estimate of the air flow rate could be used to estimate the power dissipation. Both tests were necessary because neither was entirely accurate: thermal measurements made assumptions about the air flow through the cameras, and it was not possible to fully isolate the iXon^{EM}+897 camera head current from the current drawn by its PCI card.

The lower power dissipation estimates for the iXon^{EM}+897 camera are likely associated with the fact that much of the signal processing and power management for this head is deferred to the PCI card inside the host computer. The ImagEM C9100-13 also has some functionality remote from the camera head. The ProEM 512B head, by contrast, is a self-contained unit apart from its power supply and ethernet connection.

As based on this test, the iXon^{EM}+897 camera is preferred, as it dissipates far less heat in the camera head than the other two cameras do.

The other environmental considerations do not significantly discriminate between cameras. None meet the requirement for functionality at -5 °C, however our current design concept will enclose the camera in a housing that will ensure the ambient temperature stays above freezing as well as removing waste heat. As far as liquid

Attribute	Requirement	iXon+897	ProEM 512B	ImagEM C9100-13
Max head power dissipation/W (lab thermal measurement)		42	80	untested
Max head power dissipation excluding Peltier/W (lab thermal measurement)	≤20	12	30	untested
Max head power dissipation/W (electrical measurement)		Vendor result pending	54.8 (vendor)	56.4 (vendor)
Max head power dissipation excluding Peltier/W (electrical measurement)	≤20	12 (lab, vendor result pending)	28.8 (vendor)	20 (vendor)
Operating temperature/ °C	-5 to 20	0 to 30	0 to 30	0 to 40
Operating relative humidity/ %	10 to 70	0 to 70	0 to 80	0 to 70
Storage temperature / °C	-25 to 40	-25 to 55	Unknown	-10 to 50
Storage humidity/ %	5 to 95			0 to 70
Minimum CCD temperature achieved/ °C		-85	-76	-80 (datasheet)
CCD warms when clocked at		1kHz frame rate for 10s at -85 °C	2kHz frame rate continuously at -70 °C	Untested
Fan		50 mm, quiet	40 mm high flow, can feel vibration	Unknown
Coolant		Water, possibly antifreeze	1:1 Glycol:Distilled water	Water
Coolant below dew point?		No	No	Unknown
Coolant below 0 °C?		Unknown	OK	Unknown

Table 8: Power dissipation data for the candidate EMCCD cameras.

cooling is concerned the ProEM 512B device can be cooled with a water/glycol mixture as a protective measure, but Andor and Hamamatsu have not committed to any statements regarding the use of such "antifreeze" coolants in their cameras. The ProEM 512B also has more robust cooling of its CCD while fast clocking, but cannot cool the CCD as deeply as the other cameras.

5.2.5 Latency and programming considerations

The relevant issues are summarized in Table 9.

Attribute	Requirement	iXon+897	ProEM 512B	ImagEM C9100-13
Latency for 1024 pixels, exposure end to receiver DMA interrupt /µs	<1130 (goal <790)	530	1000 to 1300 (jitter present in experimental data)	Untested
Linux support		Available	"Soon"	Available (3rd party, free). Untested by Hamamatsu
Real-time adaptability	Is necessary	Proven	Unknown	Likely
Custom clocking		By request, for fee	Editable scripts	Likely, via Camera Link commands

Table 9: Latency and programming considerations for candidate EMCCD cameras.

For a 50 Hz 3dB fast tip-tilt servo bandwidth, the worst-case latency than can be accommodated is 790 microseconds (RD2). For an equivalent 40 Hz servo, this can be relaxed to 1130 microseconds. Within this time, the system must read out the region of interest from the CCD and transfer the data to the host computer. A further 100 microseconds has been budgeted to calculate a centroid and its error in position, and send correcting voltages to the fast tip-tilt mirror. The latency of the camera hardware and the associated software must always be short enough to allow a complete servo cycle to fall within these time limits.

Some latency information could be determined with an oscilloscope and a camera driven by the vendor's demonstration software. The end of a camera exposure is signalled at a port on the camera head. All three cameras transfer data to the host computer's memory using direct memory access (DMA), after which an interrupt line is asserted on the computer's PCI bus to tell the computer that it is there. The time between these two signals is the time taken to read the CCD data, transfer it to the host, and make it available for analysis.

Both test cameras were made to repeatedly read out 1024 pixels of image data. For the iXon^{EM}+897, the hardware latency was found to be 520 microseconds, with no significant jitter. However, the ProEM 512B latency varied from 1.0 to 1.3 milliseconds. This result favours the iXon^{EM}+897, as it has a latency within our goal and negligible jitter was measured in our experiments.

The fast tip-tilt software must run as a hard real-time process, due to the tight latency requirements mentioned above. Several real-time operating systems could be used for this purpose, but none are supported by any candidate camera vendor. However, some do offer ordinary Linux support, and our group already has considerable experience developing software for Xenomai. As a result, the possibility of porting Linux camera drivers to Xenomai, or writing Xenomai drivers from scratch, was investigated.

Andor have a Linux software development kit for its cameras, which was purchased as part of our evaluation. This consisted of a closed-source user library, and some open-source camera drivers for the Linux kernel. The latter were very useful because they allowed access to the interrupt service routine, triggered by the DMA interrupt mentioned above, that processed the camera data. After some experimentation it proved possible to port this routine to Xenomai so that it ran as a hard real-time process, giving us real-time access to the camera

data. For a repeated 32 × 32 pixel readout, oscilloscope monitoring showed that the time between the DMA interrupt and the end of the interrupt service routine varied between 16 and 32 microseconds.

The ProEM 512B uses a customised low-latency ethernet stack called "iPort", licensed from Pleora Technologies. iPort is a closed-source product, and Princeton Instruments only supports ProEM512B development under Windows. To get the camera to work in Xenomai (or some other real-time operating system) it would be necessary to reverse-engineer the ethernet protocol used by iPort and to write an entire host application to perform the high-level camera communication. In their favour, Pleora has moved towards a more open gigabit camera standard known as "GigE-Vision" and provides vendors with Linux software development kits for this. Princeton Instruments has indicated they will follow this transition. However it is unclear when this will happen, or whether Pleora's drivers will remain closed to external developers.

The ImagEM C9100-13 uses Camera Link for data transmission. There are many vendors who manufacture Camera Link PCI cards with Linux support. EDT Incorporated, for example, provides semi-closed-source Linux drivers as a free download, and provides "hooks" into the code and an example program that shows how to run the cards under RTLinux (a commercial hard real-time Linux). The implementation is very similar to what the Cambridge team achieved with the iXon^{EM}+897 camera so a Xenomai adaptation appears straightforward. The Cambridge team has not tested the ImagEM C9100-13, but encouragingly Camera Link is explicitly designed to minimise latency issues. The situation is less certain in terms of higher-level configuration and control, as Hamamatsu explicitly supports only Windows and MacOSX in their programming interface, and if they are unwilling to release their control protocol then reverse engineering of their Camera Link serial channel protocol would become necessary.

The final aspect of latency we have considered is the time required to read out a subframe. The experiments described above were able to demonstrate that if two full rows of data were read out, then the latency requirements could be met. However, the successful operation of the FTT/NAS requires that a square subframe, ideally 32 × 32 pixels in size, at an arbitrary position on the CCD be read out rapidly.

All the vendors under study offer arbitrary subframe readout schemes for their cameras[3], however these inevitably perform additional time-consuming serial register shifts to ensure that no charge from elsewhere on the CCD gets added into the region of interest. The result is that for a 32 × 32 region, at best a 2 ms latency is achieved. Some vendors also offer schemes without charge clearing that are faster, but these constrain the region of interest to being situated at one corner of the CCD.

We have devised a custom clocking scheme that satisfies the latency requirement. This exploits the fact that under most circumstances the interferometric target will be by far the brightest target in the field of view of the FTT/NAS sensor. In this case charge close to the sub-region surrounding the objective point on the CCD can be summed into that region without substantive penalty, thereby minimising the additional serial register shifts. In the rare cases where other comparably bright stars are in the field of view of the camera, the FTT/NA system can be commanded to fall back to an "ordinary" sub-framing mode with a consequent reduction in temporal performance.

However, such a scheme requires control of the CCD clocking lines beyond what is offered in any candidate camera's software development kit. As a result, dialogue on the issue was taken up with the camera vendors. Andor has informed us that there are timing issues associated with readout of the CCD97, specifically that artefacts can be caused by initiating a parallel shift while the readout amplifier is on (these will apply to any of the three candidate cameras). However, if we were prepared to accept an image size no larger than 23 × 23 pixels this situation can be avoided, and they might be able to devise a clocking scheme for us, for a fee. Princeton Instruments has stated that their clocking arrangements are in their library, and that they are willing to provide the library source code to us so that we can do our own customisation. The situation with Hamamatsu is unknown, and depends on how flexible their Camera Link configuration channel is, and whether they would be willing to release the protocol for it.

[3]The ImagEM C9100-13 restricts the subarray width and height to multiples of 16 pixels.

5.2.6 Conclusions

For the FTT/NAS the most important differences between the three potential candidate cameras were their thermal dissipation, their ability to run underneath a real-time operating system, and their latency.

The Andor iXon^{EM}+897 head is preferred in all these respects, and the risk that it would not be able to meet the system requirements is low. The subframe size restriction to no more that 23 $\times$ 23 pixels is not optimal but can satisfy the top-level system requirements, and applies to the other cameras as well. The shortcomings associated with the camera shape and maximum supported cable length will be relatively straightforward to us to work around.

The Princeton Instruments ProEM 512B is a relatively high risk candidate, as the hardware latency and jitter do not meet the requirements, the likelihood of real-time operation is low and the high power dissipation greatly increases the complexity of any heat removal scheme.

The Hamamatsu ImagEM C9100-13 falls somewhere between these two in that it has intermediate heat dissipation and real-time potential. The size of its controller box is a minor disadvantage and the hardware latency has not been measured. Hence the risk that this camera will not meet the requirements is intermediate.

6 Conceptual Opto-Mechanical Design

The main objective of the opto-mechanical design of the FTT/NAS will be to meet the beam stability and the image quality requirements. As explained earlier the FTT optics arranged on the Nasmyth table, including the dichroic and the EMCCD camera, must remain sufficiently stable in tilt and displacement such that the tip-tilt zero point moves by <0.5 μm on the detector surface. The stability required of the optical components in each of the candidate layouts has been provided in a provisional budget in Table 3 of Sec. 2.5 or in the derived requirements (RD2). For the preferred layout(s) these call for tilt stability as low as 0.045 arc seconds and shear displacements of <0.5 μm over a night-time temperature change of up to 5 °C.

To meet such high stability requirements we intend that the optical components not be fitted to mounts with adjusters: instead every component, once aligned, will remain fixed in position. This in turn will require the system to be tolerant of focus changes so that any focus adjustment required be limited to a simple occasional adjustment for a seasonal change. The stability requirements also demand low sensitivity to thermal changes and so thermal gradients across component mounts will need to be minimised. This has led to us adopting aluminium rather than stainless steel for the mount material. Although Invar performs better than aluminium it is much more expensive to purchase and machine, and as such its additional cost cannot reasonably be justified.

Apart from the difficulty of holding the optical components in mounts to these high tolerances, the stability of the optical arrangement will also be heavily dependent on the foundation to which they are attached and so the likely performance of the Nasmyth optical table is a concern that we wish to raise to the MROI Project Office[4]. It is likely that the Nasmyth optical table will distort with changes in temperature. To minimise the effect of this it is proposed that the optical components are mounted on a common base-plate, supported at three points from the optical table. It is also desirable that the layout be compact and that the EMCCD camera, which is not mounted on the common base-plate, be fixed as close to the baseplate as possible.

6.1 Layout

The rationale for selecting our preferred layout (the DLT configuration) has already been presented in Sec. 4.3. In summary, the OAP layout has not been favoured due to the difficulties of maintaining a stable opto-mechnical configuration, the DT layout is compromised by its similar need for a long and unstable baseplate, leaving the DLT and zoom layouts as the two best potential candidates.

[4]We note that the FTT/NAS requirements document explicitly allows for instabilities in the Nasmyth table to be ignored from the point of view of requirement compliance. However we mention this possibility as it has arisen directly out of our analysis of the stability required to meet the FTT/NAS requirements and we feel that it is prudent that the Project Office be informed of this critical issue.

The zoom layout is the most compact and has somewhat lower stability requirements on its second lens as compared to the second fold mirror in the DLT layout. However, more importantly it allows the FTT camera to be attached to the optical table close to the fixed kinematic seat of the common base plate. This will help minimise any vertical shear between the camera and the base-plate that might occur as a result of the optical table bending due to a temperature difference between its upper and lower skins. On the other hand, the camera will still be placed very close to the edge of the optical table and the wall of the surrounding telescope enclosure.

However, we have not yet established that a suitable optical implementation for the necessary apochromatic optics can be realised, and so at the present moment the DLT layout is most likely to be adopted as the baseline design. We intend to carry out further optical design work, together with more mechanical optimisation, during the preliminary design and test phase to arrive at the most compact and stable final layout.

6.2 Mechanical analyses

6.2.1 Base-plate stiffness

Figure 3 shows the geometric arrangement for each of the four candidate opto-mechanical layouts. For each candidate layout, Finite Element Analysis was performed to obtain estimates of the natural frequency of the first mode of vibration of the common base-plate. Each model assumed an aluminium base-plate 15 mm in thickness and estimated masses for all the optical components and mounts. These results are presented in Table 10. The DT and OAP layouts have low natural frequencies but the DLT and zoom layouts have lowest eigenfrequencies well above 60 Hz and so are unlikely to be significantly excited by vibrations of the telescope or enclosure.

Layouts	**DLT**	**Zoom**	**DT**	**OAP**
First Natural Frequency /Hz	138	108	37	45

Table 10: Natural frequency of the first mode of bending of candidate base-plates.

6.2.2 Thermal expansion analyses

An analysis of the effects of thermal expansion of the Nasmyth optical table (assuming a uniform temperature distribution) has shown that the relative angular orientations of the optical components are invariant to temperature changes and only the change in focus needs to be considered. Expansion of the optical table is equivalent to a lateral shear of the beam from the telescope. The same argument can be applied to the common base-plate. As a result, as long as the optics are suitable oversized, this lateral shear will not cause any problems in the optical stability of the system.

6.2.3 Thermal gradient analyses

To establish which material should be used for the common base-plate and the optical mounts a number of finite element analyses were performed to compare the performance of stainless steel, invar and aluminium. Heat transfer parameters appropriate to natural convection, i.e. assuming little or no wind circulating in the enclosure, were included in the FEA model. These analyses confirmed that invar produced the lowest distortions but was only marginally better than aluminium. This is because any thermal gradients produced due to a changing air temperature will always be very low for these materials, and so the resulting angular deviations of the optics are always small enough to be ignored.

To give the reader a feel for the magnitude of the thermal gradients needed to exceed the FTT/NAS opto-mechanical stability budget, Table 11 shows the acceptable temperature difference between the left and right surfaces of the dichroic mount for no more than a 0.05″ tilt of the optical surface, and also the temperature

difference between the surfaces of the dichroic mount that would result from a change in ambient air temperature of 0.5 °C at one side of the mount. To compare the performance of the different mount materials a figure of merit was calculated from dividing the acceptable temperature difference by the temperature difference induced by a change in ambient air at one face of the mount. Our data show that stainless steel has only marginal performance while aluminium is a suitable alternative to invar.

FEA conditions	**Invar 36 CTE = 0.7 × 10^{-6}**	**Stainless Steel 304 CTE = 17.2 × 10^{-6}**	**Aluminium6061 CTE = 23 × 10^{-6}**
Acceptable temperature difference between surfaces that gives rise to no more than a 0.05″ tilt of the dichroic	0.05 °C	0.002 °C	0.001 °C
Temperature difference between dichroic mount surfaces produced by a 0.5 °C change in the ambient air temperature at one face	0.00058 °C	0.00049 °C	0.000056 °C
Figure of merit (ratio of above two quantities)	86	4	18

Table 11: Comparison of the surface temperature differences of the dichroic mount for two FEA conditions and three materials. Note how the temperature gradient caused by a step change in air temperature on one side of the dichroic mount is comfortably lower than the maximum allowed gradient if invar or aluminium were to be used for the mount material.

6.2.4 Earthquake loads

In our concept design the optical components will be held in mounts which are very similar in design. Only the lens mount will be significantly different and in this case the lens will be held firmly so that there should be no risk from earthquake loads. The dichroic mirror will be the largest element to manage and so the earthquake loading for other elements will be smaller. The mounts will be sufficiently rigid that their first natural frequency will be high and they can be regarded as rigid bodies for earthquake loading calculations.

The dimensions of the dichroic are expected to be approximately 120 mm × 120 mm × 15 mm. If we assume an INFRASIL (fused silica) substrate, the mass will be approximately 0.5 kg and the force produced by a 0.3 g earthquake will be approximately 1.5 N. This force is so low that either of the mount designs we have investigated (see Sec. 6.4) could be used without risk of the dichroic becoming misaligned. In the case of the "edge clamp" method, a set of retaining surfaces would be introduced to prevent excess movement of the dichroic during handling and alignment.

6.2.5 Relocation of UT

The force produced by a 0.4 g relocation shock on the dichroic would be approximately 1.5 N and 2 N for our two mounting concepts respectively, assuming the shock spectrum is similar to an earthquake. Again, these forces are so low that either mounting method could be used. During the preliminary design phase the shock loading situation will be examined in more detail to ensure that our mounts are adequate.

6.2.6 Tilt of Nasmyth table

Thermal effects acting on the Nasmyth table mounting structure may produce a shear of the table in the horizontal and vertical directions but are also likely to produce tilts about the vertical and horizontal directions (as

well as local deformations of the table surface). These latter effects will directly affect the position of the tip-tilt zero point. We have presented an example of our rudimentary analyses of the potential magnitude of these effects in Appendix B, but again remind the reader that for the purposes of meeting the FTT/NAS zero-point stability requirement the impact of perturbations in the Nasmyth table are permitted to be ignored. However, from an overall system perspective they will likely need to be addressed by the Project Office as a matter of some urgency.

6.3 Base-plate design

An example of an initial design for one of the common base-plates (for the DLT layout) is presented in Figure 8. Here again aluminium, rather than invar, has been selected as the plate material because it has excellent thermal conductivity which promotes a uniform temperature distribution. The difference in the thermal expansion coefficients of aluminium and stainless steel (the table surface material) could over-constrain the plate if it were coupled rigidly to the table and so we propose to mount it via three adjustable ball end screws. A kinematic design will be applied to the interface between the plate legs and the table so that one part will be allowed to expand or contract in an unconstrained way. One leg would be referenced at the position nearest to the FTT/NAS sensor using a cone interface while the other two legs would seat in V blocks. The two V blocks would be oriented to allow the two legs to move along lines which pass through the position of the pinned leg. In no case would the FTT camera be mounted onto the base plate: if this were so excessive heat and vibration would likely be transmitted to the optical components via the base plate.

6.4 Optical mount design

Figure 8: Conceptual diagram of the common base-plate for the DLT layout. The overall dimensions are roughly 400 mm × 300 mm.

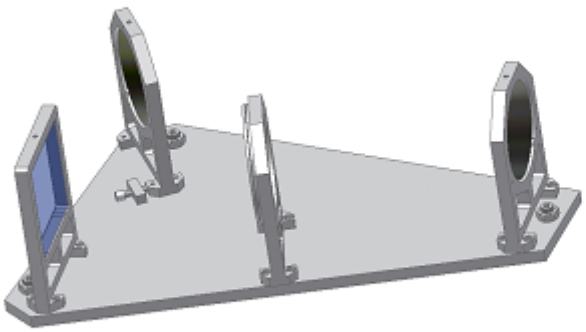

Because of the very high stability requirements placed on the position and orientations of the optical components their mounts have been designed with a symmetric light-weight structure to ensure uniform thermal dimensional change and also to minimise thermal inertia. The number of parts for each mount will be kept to a minimum in order to simplify the interfaces and reduce thermal resistance. Off the shelf adjustable mirror mounts are generally not suitable for high stability applications because they present complex interfaces and the typical use of differing materials can degrade thermal stability. Therefore the components which would be used to adjust the optical mounts for any initial alignment purposes will not be included between the optic and

the mount but at the interface between the mount and the base-plate and in such a way that they will not remain in contact once the mount has been positioned and bolted down.

The material for the mounts of the optical components has been chosen to minimise temperature differentials and thus distortion when the ambient temperature varies. Invar 36 or super-invar has excellent performance due to its near zero CTE but it has much poorer thermal conductivity than aluminium. The costs for invar (both purchase and machining costs) are a factor of 2-3 times greater than for stainless steel and at least 5 times higher than for aluminium alloy. Furthermore, invar does not have good corrosion resistance properties. On the contrary, aluminium has excellent thermal conductivity, is cheap to procure and machine, and can be easily passivated. On these grounds we have selected it as the material of choice for the mounts of the optical components and the common base plate.

6.4.1 Dichroic mount

The dichroic is required to have a tilt stability of $\leq 0.045''$ over a temperature change of 5 °C. Due to the difference in CTE between the dichroic material (INFRASIL) and the aluminium alloy of the mount, there will be relative movement between the dichroic and the mount if the temperature changes. Any tilt of the dichroic due to this movement must be minimised by careful design of the mount and the clamping method used to hold the optic. Two methods for clamping the dichroic are proposed and these are depicted schematically in Figure 9. These two basic favoured approaches are:

1. The use of two point/line contacts to support the lower edge of the dichroic while a spring load is applied from the top – panel (a);
2. The use of three point/small area contacts on one face of the dichroic, as depicted in panel (b). In this scenario the contacting faces must be located in the plane passing through the centre of the frame to eliminate any tilt of the dichroic should a temperature gradient develop between the top and bottom of the mount.

In method 2, the tilt of the dichroic could change if there were any differential movements between the contacting surfaces, e.g. due to temporal changes in any dust or corrosion at the interfaces, whereas for method 1 the relative movement between the dichroic and the mount should only induce small second order errors. In both schemes the dichroic would be seated in a position within the mounting frame which would be chosen to minimise any tilts due to temperature gradients and would include a retaining shoulder or retaining tabs so as to prevent excess movements of the optic during an earthquake or telescope relocation.

During the preliminary design and test phase of the project further FEA will be carried out on the mount design and interface with the optical components. At least one type of mount will be manufactured and tested for stability with temperature and over periods of up to 12 hours to simulate the longest night.

6.4.2 Focus lens mount

The lens mount will be designed so that the lens remains centred in the mount to within 0.35 µm vertically and 0.47 µm laterally over a temperature change of 5 °C. Any tilts of the optic and mount must be $\leq 0.7''$ over the same temperature change. Maintaining this level of stability will require careful design of the interface between the lens and the aluminium mount and the conceptual design we have adopted is similar to the methods used in holding optics in cryostat applications. This is shown schematically in Figure 10. The lens would be held circumferentially at its edge by aluminium fingers which project from an aluminium centering ring. The fingers provide sufficient compliance to account for the different CTEs of glass and aluminium. The centring ring is screwed to the aluminium mount so that the lens projects into a recess bored into the mount. A retaining ring, machined with a shoulder that projects through the first ring, is screwed to the mount through clearance holes in the first ring. Compression springs are fitted to these screws so that the retaining ring is pre-loaded against

Figure 9: Conceptual designs of the dichroic mount with different clamping methods: (a) mount bearing on the edge of the dichroic, and (b) mount bearing on the face of the dichroic.

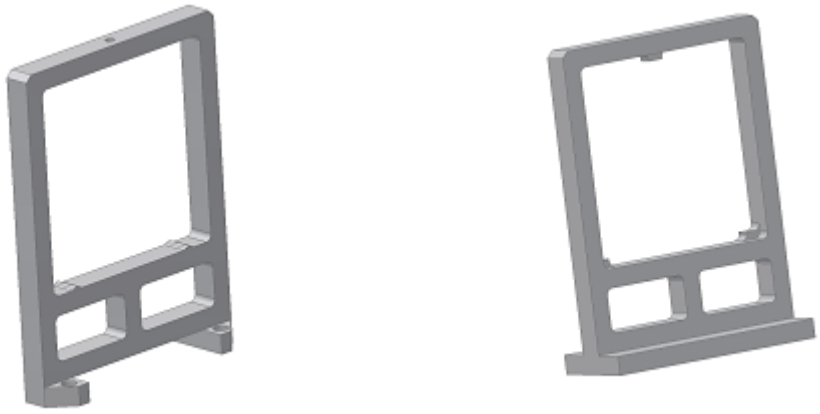

the lens and retains the lens against a shoulder machined in the recess of the mount. The contacting surface of the shoulder machined in the mount and the retaining ring are precision machined so as to be tangent to the lens surface.

This type of mount can be adjusted in azimuth using temporary adjusters fitted to the base-plate. Manufacturing tolerances will be controlled so that the mount should not need to be adjusted in tilt and can be bolted directly to the base-plate, once aligned.

6.4.3 Folding mirror mounts

Figure 10: Focus lens and mount. The lens clamping method is designed to maintain the lens centrally in the mount to within 0.4 μm over temperature changes of up to 5 °C. A cemented lens design has been assumed.

The folding mirror mounts have a requirement on stability similar to that of the dichroic, i.e. between 0.05″ and 0.1″ over a temperature change of 5 °C. The reflecting surface of the mirror must also not move normal to its plane by more than about 0.3 μm to 0.5 μm over the same temperature change. The design of our proposed mount is based on the same principles as the dichroic mount although the mirror is expected to be circular. For manufacturing purposes and to maximise stability, both mirror mounts might be identical even though the beam is smaller for the mount closest to the CCD camera.

6.4.4 Corner cube mount

A suitable commercial corner cube mount will be tested during the preliminary design and test phase. The stability requirements for the corner cube are orders of magnitude less stringent as compared to the components discussed above – typically fractions of a millimetre as opposed to microns – and so we believe a COTS mount is likely to be sufficient.

6.5 Camera mount

We intend to contain the FTT/NAS camera within an enclosure in order to control its environment. However, it remains desirable that the camera support experiences the same thermal environment as the optical component mounts since this will help ensure that any changes of height with temperature are similar for the whole optical system. Such a scheme would minimise any temperature induced drift of the tip-tilt zero point on the CCD. The camera mount will therefore be outside the camera enclosure with the camera connected by stiff rods which pass through the enclosure insulation. To prevent heat transferring from the camera to the mount the rods must also provide thermal isolation. Our proposed camera mounting arrangement is shown in Figure 11. The camera body is clamped onto a small interface plate via the mounting holes provided in the stainless steel chassis at the front of the camera. This plate is connected to the camera mount using carbon fibre reinforced tubes which pass through holes in the front wall of the camera enclosure. These tubes are good thermal isolators and are very stiff. Thermal FEA shows that the carbon fibre tubes are very effective in reducing heat transfer from the camera to the support.

Since it is important that dry air be retained within the enclosure, adequate seals will be produced where the tubes pass through the insulation. Another tube forms a barrel so that the incoming light beam can pass through the insulation to the CCD window.

The camera mount will be made of aluminium and must interface to the Nasmyth table which has a stainless steel skin without introducing any over-constraints when the temperature changes. To prevent over-constraining the camera mount we intend to bolt it down firmly at the centre of the base flange but clamp it with preloading springs and screws at the outer edges of the flange. The “wings” at either side of the mount which project behind are primarily provided to prevent the camera from tilting backwards when the hold-down bolts are removed from the base flange but can be used to help position the camera using adjuster blocks.

6.5.1 Earthquake and relocation load

None of the camera manufacturers specify shock load limits. Although we have asked each specifically, only one manufacturer has responded so far and has confirmed that they have no information available. There is no reason to believe that the camera will not survive an earthquake load of 0.3 g but, when mounted to the optical table the actual shock load will depend on the earthquake spectrum and any magnification introduced by the table mounting structure. We do not expected this to be an issue though.

Shock loading due to relocation, although only quoted to us as 0.4 g, will depend again on the shock spectrum and this is likely to contain higher frequency components than an earthquake. Relocation loading will be assessed during the preliminary design phase and a conclusion reached as to whether to recommend that the camera be dismounted or left in place during relocation.

6.6 Seasonal Focal adjustment

The operating temperature range for the FTT/NAS is required to be between -5 °C to 20 °C with a goal of operating down to -10 °C. The image quality requirement allows for a range of de-focus of roughly ±300 µm. However, a seasonal adjustment of focus may be required, depending on the final optical design and layout. For stability reasons, it is not intended that any critical part of the FTT system will have focus actuating elements. If

Figure 11: Design of the FTT camera mount (a) showing the temperature control enclosure, and (b) with the enclosure removed.

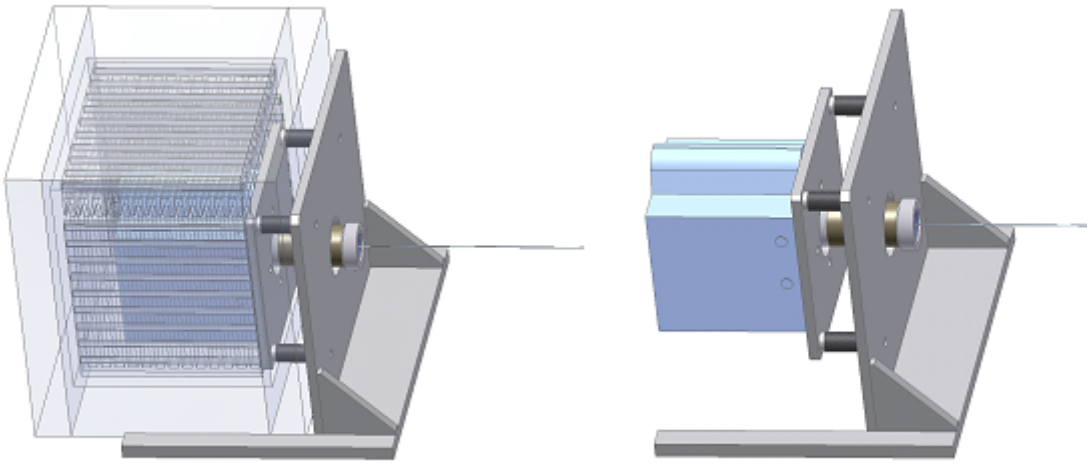

focus adjustment is required this will be done either by repositioning the final fold mirror by a small deterministic amount, by placing a window of different thickness over the camera aperture or by using a motorised slide located between the final fold mirror and the camera which carries two glass plates of different thicknesses.

6.7 Beam alignment

The mounting holes in the base of each optical component mount fitted to the common base-plate will have sufficient clearance so that the mount can be rotated slightly in azimuth. Fine pitch adjusting screw blocks will be provided for alignment purposes, as shown in Figure 12 but will be backed-off or removed after the mount has been positioned and bolted down. Manufacturing tolerances will be set so that no tilt adjustment is necessary at the base of the mount. Once all of the optics is aligned on the base-plate it will only be necessary to position the camera and adjust its horizontal shear and tilt about the vertical axis before bolting it down.

7 Conceptual Thermal Design

7.1 Thermal control

The vendor-specified minimum guaranteed operating temperature for all the candidate cameras is 0 °C, in a non-condensing environment. The minimum survival temperature for the Andor and Princeton cameras is minus 25 °C but for the Hamamatsu camera it is only -10 °C. Therefore for operational and camera safety reasons the FTT/NAS camera will be placed within an enclosure in which the air will be maintained above 0 °C. To prevent overheating of the camera and to meet the maximum surface temperature constraints for hardware that is located in the telescope dome, the camera enclosure must be insulated and heat will need to be removed from it. This concept requires that some further design constraints be applied:

1. When operating at night the camera enclosure temperature must be controlled to protect the camera and to minimize heat dissipation to the environment, and to ensure that the outer surface temperature of the camera enclosure is within 2 °C of ambient;

2. The camera environment should be controlled at all times, even though the camera may not be switched on. This will ensure that the camera can be switched on without first having to warm up or dry the

Figure 12: Detail of the common base-plate showing a conceptual screw block for adjustment of the azimuth of the final fold mirror.

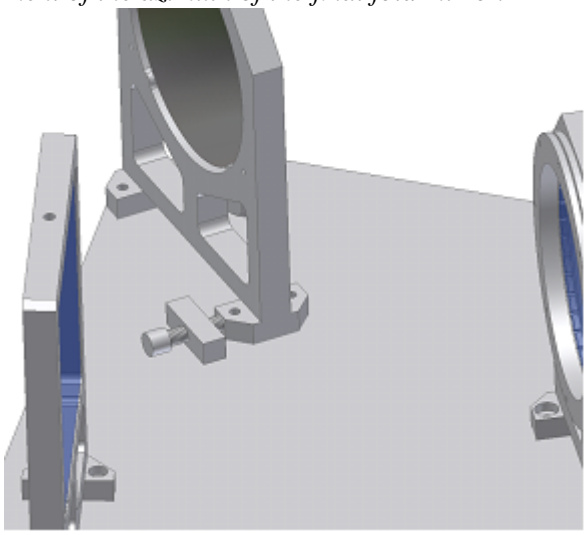

enclosure;

3. The camera enclosure should contain a heating element so that the enclosure can be warmed up after a long power break during cold weather;

4. The air in the camera enclosure should be maintained above the dew point whenever the camera is powered on (and preferably at all times so as to reduce the risk of condensation on the internal electronics);

5. Heat will need to be removed from the camera Peltier heat exchanger and the enclosure. We intend to exchange this to a liquid flowing at a controlled temperature and flow rate.

These constraints will be satisfied by a thermal control system, managed by the FTT/NAS computer. The major components of this system are illustrated in Figure 13. The camera enclosure will be fitted with temperature and dew-point sensors connected to a custom interface board in the FTT/NAS electronics interface rack mounted in the EIE electronics housing designated Q5. A thermal control panel or enclosure, to be located on the telescope enclosure wall beneath the Nasmyth optical table, will supply fluid at a controlled flow rate (and possibly temperature) to the camera enclosure. The FTT/NAS electronics will then interface these monitor and control signals to the FTT/NAS computer which will control the operation of the thermal system to ensure camera safety.

7.1.1 Camera enclosure analysis

In the following paragraphs we present a thermal analysis for the preferred FTT/NAS sensor, the Andor iXon^{EM}+897. Manufacturer's specifications for the dissipation of this camera are not generally available and so some tests were carried out during our camera evaluation period to establish where heat was being dissipated. These results are shown in Table 12.

Residual heat dissipation The residual heat dissipated in the camera head will be that heat which is dissipated by the control and interface circuits located in the camera body, and which is vented through slots in the case. This heat is not removed by the Peltier liquid cooling circuit. Since the fan within the camera cannot be used because of vibrations, the residual heat can only circulate within the camera enclosure and only a small fraction of it will be removed by conduction to the Peltier cooling block. The residual heat was estimated by measuring the temperature of air escaping from the camera body with the fan operating but with no Peltier operation.

Figure 13: Block diagram of FTT/NAS camera thermal control system. The camera enclosure is located on the Nasmyth optical table; the electronics interface and FTT/NAS PC would be located in the EIE electronics housing designated "Q5"; and the flow control panel (or enclosure if necessary) would be located beneath the optical table.

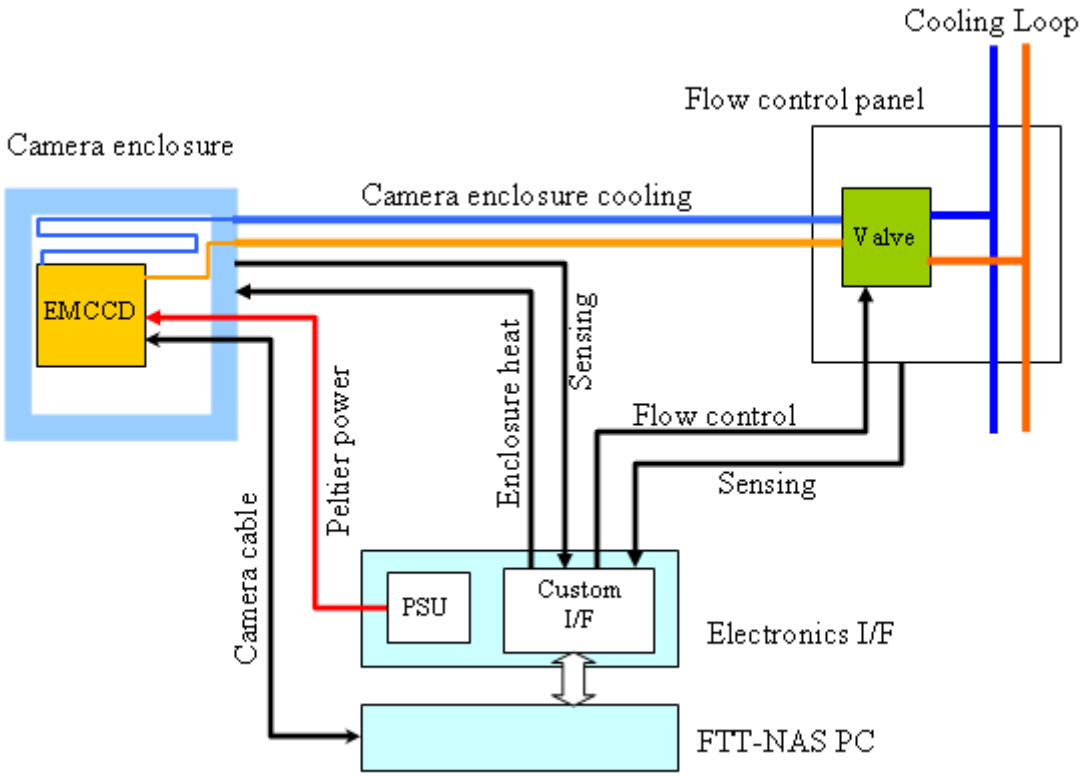

	Andor iXon^{EM}+897	
Power supply	To camera interface by PCI bus & PC PSU; to Peltier by separate PSU module	
Power consumption	71 W (calculated from figures given)	
Power dissipation	**At Camera**	**In EIE electronics housing**
Residual power	12 W (measured at camera)	26 W (PCI board)
Peltier power (max)	30 W (Peltier supply)	~3 W (estimated efficiency of PSU)
Total Power Dissipation	42 W	29 W

Table 12: Power dissipation estimates for the Andor iXon^{EM}+897 camera head.

The dissipation measured with the Andor camera was between 8 W and 12 W depending on the assumed efficiency of the fan. The dissipation quoted to us for the Princeton and Hamamatsu cameras was 30 W and 20 W respectively.

Allowable residual heat estimate An estimate of the heat flux which may pass through the walls of the camera enclosure without the surface temperature increasing by more than 2 °C can be obtained from Newton's law of cooling. For the purposes of this estimation we have assumed the following:

1. That there is no forced cooling (e.g. provided by any wind);
2. That the enclosure has outer dimensions or 340 mm high × 340 mm wide × 300 mm deep (area = 0.64 m^2)
3. An average convective heat transfer coefficient h_c of 2.1 over the whole surface area for a $\Delta T = 2$ °C
4. That any radiative cooling is insignificant.

In this case we can write for the total heat flux, Q:

$$Q = h_c A (T_1 - T_2) = 2.1 \times 0.64 \times 2 = 2.7 \text{ W}.$$

We have estimated the contribution from radiative heat flux using an on-line thermal system calculator. Assuming the camera is sandwiched between surfaces which are 2 °C cooler than its enclosure, the additional heat flow through the walls of the enclosure will be roughly 3 W. Therefore in calm conditions the allowable heat flux, accounting for natural convection and radiation, will be 5.7 W.

If the air around the camera has a mean velocity of 1m/s then the convected heat flux can increase to approximately 6 W for a 2 °C surface temperature difference, increasing the total heat flow allowed through the enclosure walls to approximately 9 W.

Residual heat removal To keep the camera enclosure surface temperatures within 2 °C of ambient in calm conditions approximately 6 W would need to be extracted using some kind of internal heat exchanger. Since forced cooling by fan is not recommended this is best done with a substantial ΔT between the internal enclosure air and liquid-cooled cold plates. This will make any heat exchange more efficient and drive convection within the camera enclosure. To ascertain what area of cold plate and range of coolant temperature would be needed to remove sufficient residual heat a simple lumped-parameter thermal model was developed.

Thermal model The simple thermal model shown in Figure 14 was constructed using equivalent capacitors and resistors to represent the thermal capacitance and resistance of the camera, enclosure and cooling hardware. The camera has a thermal capacitance, C_c, determined largely by the mass of its metal chassis, and a convective thermal resistance, R_{ce}, to the air in the enclosure determined by its surface area and a convective heat transfer coefficient. The enclosure air has a small thermal capacitance, C_e, and the enclosure material has a thermal resistance, R_{ins}. Appropriate convective heat transfer coefficients for enclosure air to inner surface and ambient air to outer surface provide thermal film resistances of R_{if} and R_{of}. A thermal radiation resistance R_{or} is placed in parallel with the outer surface convective heat transfer resistance. It is based on an average shape factor for the surfaces and surroundings, a 2 °C temperature difference between surface and surroundings and a linearization of the relationship at 278 K (5 °C). Heat transfer from the enclosure air to the cold plate is through a thermal resistance R_{pe} which depends on the area of the plates and a suitable heat transfer coefficient. The aluminium cold plates have a thermal capacitance, C_p, and a thermal resistance, R_{pf}, to the fluid flowing through them. The cooling fluid has a thermal capacitance and a resistance based on its specific heat and mass flow rate.

Estimation of model parameters Our calculations of the equivalent thermal capacitances and resistances used in the thermal model of the camera enclosure are tabulated in Table 15 and Table 16 in Appendix A.

We assumed that the enclosure had outer dimensions of 340 mm × 340 mm × 300 mm and had insulating walls 40 mm thick. Three finned aluminium cold plates provide a large surface area coupled to the coolant pipes through a much smaller surface area. Convective heat transfer coefficients were calculated for each surface using standard heat transfer calculations. These were linearised at the expected temperature differentials to provide thermal resistances. The coolant assumed was a 50% water/glycol mix with a flow rate of 1 litre per minute.

Figure 14: An electrical analogue of a lumped-parameter thermal model for the camera enclosure. It features thermal masses (capacitances) for the camera, enclosure air, cold plates and cooling fluid; thermal resistances for convection at surfaces, the enclosure wall insulation and the cooling fluid; and assumes that 10 W of residual heat is dissipated in the camera.

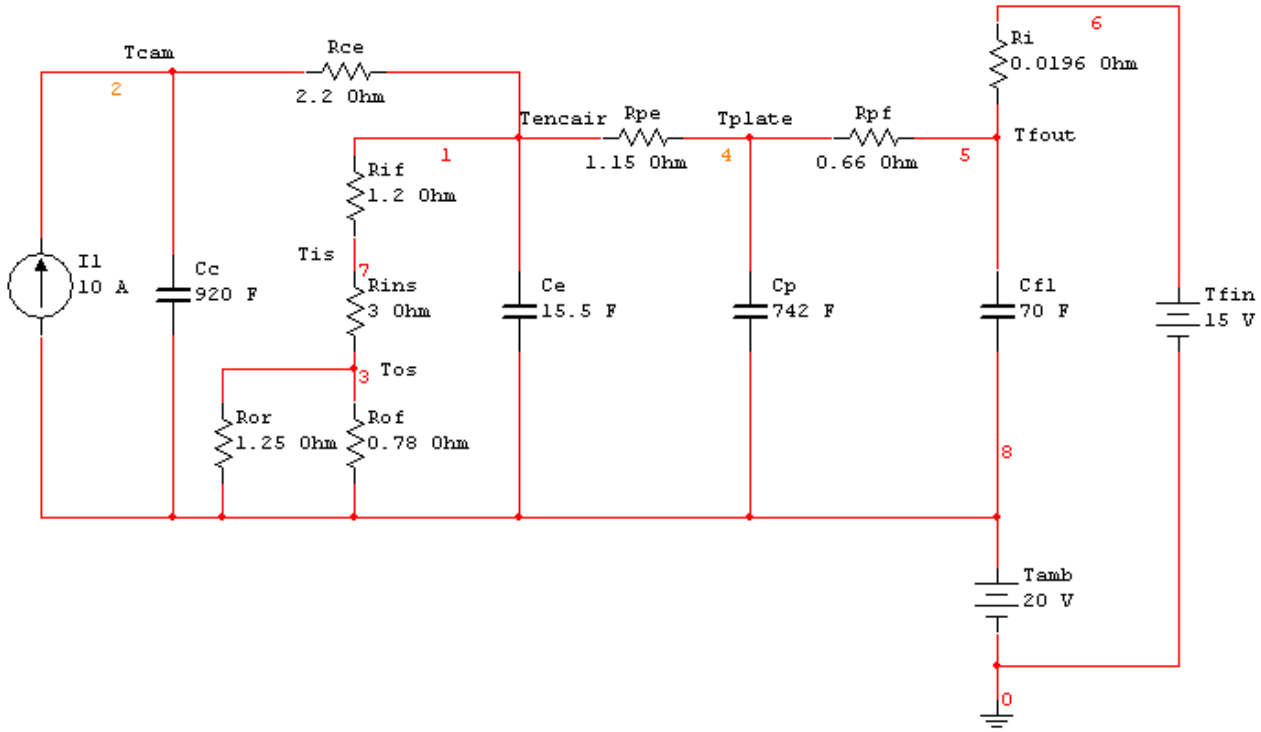

Results from thermal model simulations Simulations using the model were performed over an ambient temperature range of -10 °C to +20 °C with the coolant temperature set 5 °C below ambient but with a lower limit of 2 °C. This is characteristic of the EIE electronics enclosure cooling loop. The alternative cooling loop, used for cooling the telescope motors at night or the enclosure during the day operates similarly but with a lower limit of -20 °C.

The results of the simulations are listed in Table 13 and show the temperatures of components and air within the enclosure, the enclosure external surface temperature and the heat flow through the enclosure wall and heat removed by the fluid.

Discussion of thermal simulation results At the maximum operating environmental temperature of 20 °C the camera chassis temperature will be 51.6 °C and the enclosure air temperature 29.6 °C; the cold plate temperature will be 20.4 °C and the coolant outflow temperature will be 15.16 °C for an inflow temperature of 15 °C. Importantly, the outer surface temperature of the camera enclosure would be 21 °C, which meets the requirement that $\Delta T \leq 2$ °C. In this case the heat removed by the fluid would be 8 W and the heat escaping

T_{amb} /°C	T_{flin} /°C	T_{flout} /°C	T_{cam} /°C	T_{encair} /°C	T_{plate} /°C	T_{is} /°C	T_{os} /°C	Fluid heat flow /W	Wall heat flow /W
-10	2	2.10	33.8	11.8	5.6	6.2	-7.76	5.3	4.6
-5	2	2.12	35.2	13.2	6.2	8.5	-3.13	6.1	3.9
0	2	2.13	36.6	14.6	6.7	10.9	1.50	6.9	3.1
5	2	2.15	38.0	16.0	7.2	13.2	6.13	7.7	2.3
10	5	5.16	41.6	19.6	10.4	17.1	10.98	8.0	2.0
15	10	10.16	46.6	24.6	15.4	22.1	15.98	8.0	2.0
20	15	15.16	51.6	29.6	20.4	27.1	21.0	8.0	2.0

Table 13: Results from simulations for ambient temperatures from -10 °C to +20 °C and with the electronics housing cooling loop. T_{is} and T_{os} are the camera enclosure wall inner and outer surface temperatures respectively.

through the enclosure wall 2 W. The enclosure air temperature is very close to the maximum environmental temperature for the camera and therefore, according to this coarse simulation, either the cooling must be made more efficient, for example by increasing the surface area of the cold plates, improving fluid coupling to the cold plates or by reducing the temperature of the cooling fluid. Changing the flow rate of the fluid has very little effect.

At the minimum operating temperature of -5 °C, the outer surface temperature of the enclosure is still within 2 °C of ambient, at -3.13 °C. And at the operating temperature goal of -10 °C, the outer surface temperature of the enclosure would only be 2.3 °C above ambient, at -7.76 °C.

These results indicate that, depending on the efficiency of the heat exchange within the camera enclosure, it may be possible to use the electronics housing cooling loop directly by incorporating a flow-controlled by-pass loop. There would be no need for any subsidiary cooling loop, pump and heat exchanger. This solution has the distinct advantage that the fluid that passes through the cold plates and then through the camera to remove the Peltier heat would never fall below 0 °C.

The cooling loop for telescope motors/daytime air conditioning is set at T_{amb}-5 °C between limits of -20 °C and +15 °C. This does not solve the problem with the enclosure maximum air temperature but would help decrease the surface temperature difference at -10 °C. However it would not be possible to use this loop to remove heat from the camera because of the risk of damaging the Peltier block and vacuum seal.

Potential solutions for camera enclosure cooling will depend on the actual residual heat from the camera and the true performance of the heat exchanger within the camera enclosure. On the basis of the results presented here the following solutions could be considered:

1. Increasing the efficiency of the enclosure heat exchange by increasing the cold plate area. There is space to do this as well as to add more fins without increasing the enclosure dimensions. If the cold plate surface area is doubled then the enclosure air temperature reduces to 26 °C;

2. Shutting off the camera in the event the internal air temperature reached 30 °C. This may be a reasonable course of action as it is very unlikely that the operating temperature would be as high as 20 °C while the camera is being used for night-time operations;

3. Using the telescope motor cooling loop but with a fluid/fluid heat exchanger so that coolant temperature to the camera enclosure can be better controlled. According to the thermal model a cooling fluid temperature of T_{amb}-10 °C would result in a maximum enclosure air temperature of 26 °C. This approach would require a much more complex cooling system and so is less desirable.

A more detailed and refined thermal model of the camera and enclosure is being developed in Matlab and will be used to guide the design of the camera enclosure in conjunction with prototype tests in the next design phase of our activities.

7.1.2 Control enclosure analysis

The power consumption requirement for the FTT/NA system is $\leq$ 250 W. It is not clear whether this is also a limit on dissipation within the EIE electronics housing. From Table 1, the total power dissipation for the Andor camera system is expected to be 71 W and since 180 W has been reserved for the FTT/NAS computer and its interfaces, this leaves no additional capacity for an additional heat exchanger and thermal controller. However, only 29 W of Andor camera power is being dissipated in the EIE electronics housing and so ~40 W of dissipation would be available for additional thermal control electronics if needed. This is more than adequate and so there are no thermal issues within the EIE electronics housing if the Andor camera is used.

If one of the other candidate cameras were to be selected then a further 70 W of power consumption (and dissipation) would need to be added to the electronics housing.

An additional 50 W of power consumption may be required for thermal control if a heat exchange enclosure is located beneath the Nasmyth table.

7.1.3 Conceptual design of thermal control

Baseline design The preferred approach to cooling of the camera enclosure and the camera itself is to use the EIE electronics housing cooling loop (referred to as Loop 1). Connections to this loop will be brought to an interface at the south edge of the Nasmyth optical table. Here a flow valve, controlled by the FTT/NAS computer in the Q5 electronics housing, will provide an appropriate flow through the camera enclosure and camera.

Temperature sensors and a dew-point sensor within the camera enclosure will be monitored by the FTT/NAS computer so that conditions can be evaluated and the camera protected as necessary.

Temperature sensors will also be placed on the external enclosure surface to monitor that it remains within 2 °C of ambient. The telescope enclosure temperature and dew point will be supplied to to the FTT/NAS by the ISS.

A small heating element will be placed within the enclosure so that it can be warmed (more quickly than the cooling loop could achieve) in the event that the system had been shut down for some time during the winter and the enclosure temperature and camera fall below 0 °C.

Finally, the camera enclosure would be reasonably sealed and fed by a constant stream of dry air at < 1 litre per minute so that the dew point should always remain at least 5 °C below the enclosure temperature.

Alternative design In the event that a greater temperature difference is required between ambient and the cooling fluid supplied, a subsidiary cooling loop will be designed. This cooling loop would exchange heat to the telescope motor/enclosure cooling loop in a separate housing mounted to the UT enclosure structure underneath the Nasmyth optical table. The components of this system would be:

1. Insulated enclosure;
2. Peltier liquid-liquid heat exchanger;
3. Circulating pump;
4. Expansion tank;
5. Flow control;

6. Thermal controller;
7. Interface to FTT/NAS computer.

7.2 Enclosure thermal design

7.2.1 Camera enclosure design

Our proposed camera enclosure is constructed on an aluminium framework which is faced with thermal insulation panels and an outer skin. The insulation properties must be very good if the enclosure size is not to become too large. It is proposed that "aerogel" insulation sheets be used as these can provide a thermal conductivity of 0.02 W/mK or lower. The overall dimensions are expected to be about 350 mm high (including a 10 mm high foot to space the body of the enclosure from the Nasmyth optical table) by 340 mm wide by 300 mm depth. The thickness of insulation would be approximately 40 mm. These dimensions leave a clear space about the camera at the sides and the top for cold plates with finned heat sinks to be fitted. The thermal enclosure is shown schematically in Figure 15. The camera is located inside the enclosure with its front mounting plate close to the front wall where it is supported by insulating supports that pass through the wall to the camera mounting bracket outside. Thus the camera is not mounted to the enclosure and the enclosure is fixed independently to the optical table. This reduces the influence on the camera of forces acting on its enclosure. The enclosure is fitted with three cold plates which are coupled in series so that cooling fluid flows through them in turn and then into the camera. Each cold plate has an integral continuous looped cooling tube and is commercially available. The finned heat-sinks will be chosen so that the total area is sufficient to produce the desired cooling capacity. The fins would be arranged so that they support natural convection from the top and sides of the camera, creating circulation of the air as far as possible.

The rear face of the enclosure would be removable for access to the camera electrical connections. The enclosure chassis will support an interface manifold in such a way that the connections for the cooling circuit are on the outside, projecting through a cutaway in the rear panel. A dry air supply and connectors for enclosure sensors will also be provided to this interface. It should only be necessary to remove the rear panel if it is intended that the camera cable should be unplugged for some reason. Otherwise all connections would be available outside the enclosure.

To minimize the increase in outer surface temperature (due to residual heat within the enclosure not being removed by the cooling system) the camera enclosure outer surface will be designed with a relatively high emissivity. Also, the cover placed over the Nasmyth table (for physical protection and to shield the table from the cold night sky) should have a similar emissivity towards the camera enclosure.

7.2.2 Camera enclosure sensors

Apart from providing temperature and humidity measurements within the enclosure for safety reasons there are sensors for monitoring the thermal performance of the enclosure. The minimum set of sensors within and external to the camera enclosure will be:

- Camera case temperature sensor;
- Enclosure air temperature sensor;
- Cold plate temperature sensor;
- Internal dew point sensor;
- External surface temperature;
- External air temperature.

In addition there may be sensors to monitor the surface temperature of the Nasmyth optical table.

Figure 15: View of the camera enclosure with the rear insulation panel removed. The overall size of the enclosure is 340 mm tall by 340 mm wide and 300 mm deep and has insulation panel thickness of 40 mm. The camera is surrounded on three sides by finned cold plates which are connected in series with the camera Peltier cooling connections. The loops of the cold pipes running through the cold plates are shown in section. The camera is mounted to a bracket outside the enclosure using insulated studs which pass through the insulation. The enclosure fixes to the Nasmyth optical table.

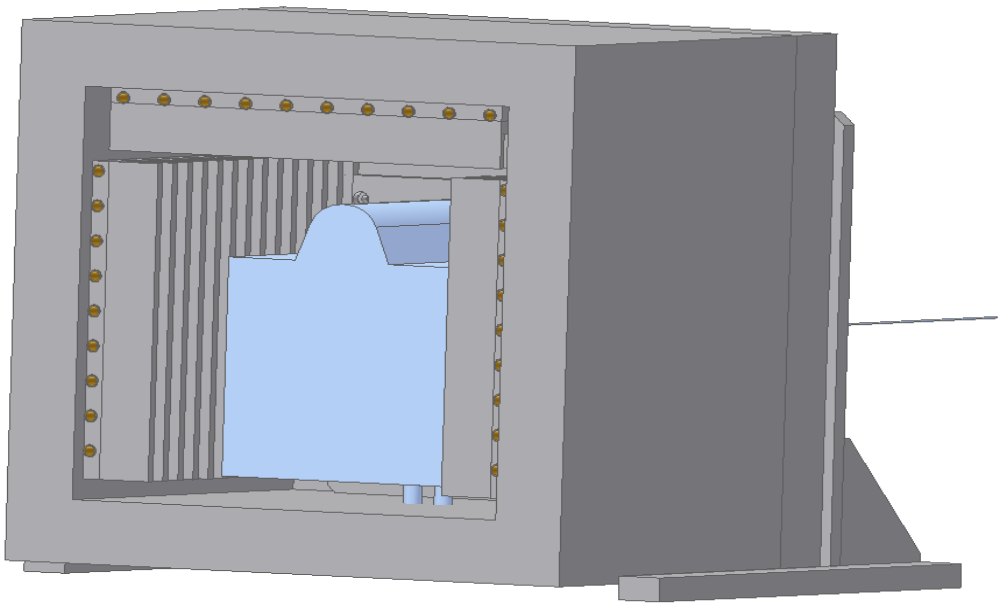

7.2.3 Electronics Housing thermal design

For the designs presented here there are no thermal design implications for the electronics housing.

7.2.4 Additional heat exchange enclosure design

If it becomes necessary to incorporate an additional heat exchanger as described in Sec. 7.1.3 then the design of this will be addressed during the preliminary design and test phase. A location has been identified for such a heat exchanger and it is likely to be placed in an insulated housing. Most of the heat generated within this enclosure will be cooled by the cooling system to which it connects and so no thermal issues are likely to arise.

7.2.5 Power consumption

The power consumed by the Andor iXon^{EM}+897 camera should just meet the power consumption requirement when combined with the other components of the FTT/NA system in the EIE electronics housing. However, if an additional thermal heat exchanger is required to cool the camera and enclosure an increase in power consumption will be necessary, though it should meet the enhanced power consumption allowance proposed in the derived requirements.

7.3 Interfaces

Interfaces to the camera enclosure have been described already and interfaces to the FTT/NAS computer are discussed in Sec. 8. The only other interface proposed for this concept is concerned with the supply of dry air. The telescope enclosure air supply is not guaranteed to be dry and so an air drying facility will be designed and fitted within the enclosure near to the Nasmyth optical table.

8 Conceptual Electronics Design

The FTT/NA system computer, the interface or controller for the EMCCD camera and the interface for monitoring and control of the FTTA are to be mounted in the equipment rack designated Q5 in the EIE UTE interface document. In addition to these functions, interface electronics will also be provided to control the thermal environment of the FTT/NAS sensor and the heat exchange mechanism which removes heat from the camera enclosure and exchanges it into the liquid cooling circuit provided within the UT enclosure. The flow valve regulating the flow of coolant to the camera will not be mounted in the Q5 electronics housing but will be located in a special housing mounted to the UTE wall beneath the Nasmyth optical table.

Each candidate EMCCD camera has different interface and power supply arrangements which take up differing amounts of space in Q5 and this conceptual design allows flexibility for any of the cameras to be incorporated.

The electronics interface will be contained in two racks mounted in Q5. A 2U rack will be used to house the computer and a 3U rack will house all other necessary interfaces and power supplies.

8.1 Computer interface

The computer is a commercial off-the shelf 2U rack-mounted Intel-style PC, to be placed within the 5U-high space allocated in equipment rack Q5. It has space for at least three interface cards, which communicate with the computer via the PCI bus as shown in Figure 16. These three cards will be :

1. An analogue to digital conversion card with digital input/output lines. This will provide a route for digitising the tip-tilt mirror position monitoring signals and analogue environmental sensor quantities prior to computer processing;
2. A digital to analogue conversion card with additional digital input/output lines. This will provide a mechanism for computer control of tip-tilt mirror position, analogue thermal management devices and possibly digitally controlled actuators;
3. A camera interface card, to interface with the EMCCD camera. This would be a custom card, a dedicated gigabit ethernet card, or a Camera Link card depending on which camera is chosen.

There are many cards on the market that combine analogue and digital input and output functions onto a single board, however, splitting these functions between the two units minimises the rework involved should one board or the other become obsolete during development.

The PCI cards will be connected to the 3U interface rack via whatever multi-core cables are dictated by the PCI card external interfaces. For added flexibility, USB, RS232 and ethernet interfaces will also be available for direct connection to the fast tip-tilt hardware if necessary.

8.2 Electronics Interface

The electronics interface will be a 3U rack containing a custom electronics interface board, interface modules, as necessary, and the FTT/NAS sensor controller or power supply, depending on the camera selected. This is shown schematically in Figure 16 and has the following features:

Figure 16: Schematic of the FTT/NAS electronics

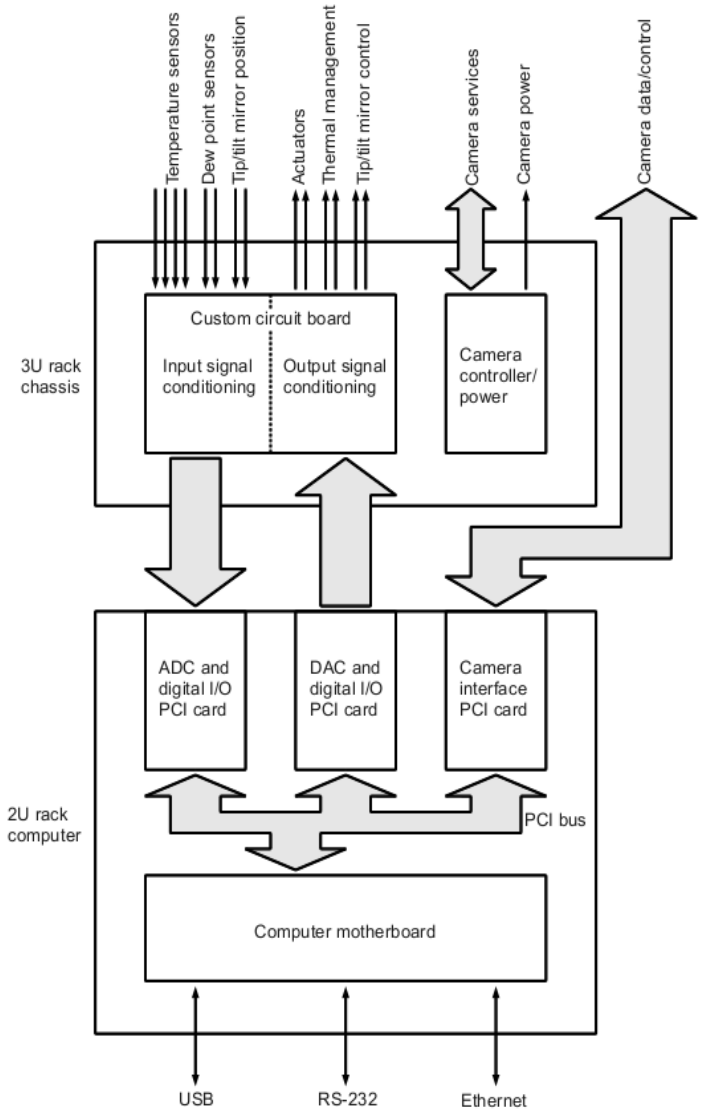

- Camera control and data from the camera are connected directly to the computer. This would be to a PCI board in the case of an Andor camera, via Gbit Ethernet in the case of a Princeton camera, or to a Camera-link PCI board in the case of a Hamamatsu camera;
- Camera control and/or power would be mounted in the 3U rack for convenience. These would be simple power supplies in the case of Andor or Princeton cameras or a special camera controller box in the case of a Hamamatsu camera;
- Input and output signal conditioning would be provided on a custom designed board mounted in the rack with connections to individual connectors on a back-panel for ease of interfacing to the various sensors or systems. A space would also be available in the rack to mount signal conditioning modules for some sensors if they are needed to deliver better performance.

8.2.1 Custom electronics interface

The custom electronics interface contains signal conditioning circuits to handle sensor inputs and control outputs. A provisional list of functions it would need to handle is as follows:

1. Interface and signal conditioning requirements for all thermal control sensors and signals connected to the camera enclosure including:
   (a) Camera case temperature sensor;
   (b) Enclosure air temperature sensor;
   (c) Cold plate temperature sensor;
   (d) Dew point sensor;
   (e) Heating element to warm up the camera enclosure following a long power-off condition in winter.
2. Interface and signal conditioning requirements for all thermal control sensors, signals and actuators connected to the camera heat exchange enclosure. This will likely include the following (according to the heat exchange system adopted):
   (a) Coolant inlet and outlet temperature sensors;
   (b) Flow control valve set point;
   (c) Flow rate sensor;
   (d) Temperature set point;
   (e) Enclosure air temperature.
3. Temperature monitoring signals from the Nasmyth optical table. These would include the following locations but might be extended if further, more accurate, temperature monitoring of the Nasmyth optical table is desired:
   (a) Nasmyth optical table temperature (in vicinity of camera);
   (b) Temperature of common base-plate;
   (c) Temperature of overhead shield.
4. FTTA demand signals to FTTA controller (also in Q5);
5. FTTA position monitoring signals from FTTA controller;
6. Actuator control signals for any focus adjustment component incorporated into the design.

It is possible that some of the sensors may be interfaced using USB or some other interface standard that would reduce the number of connections to the custom electronics interface. This would probably involve increased heat dissipation on or near the Nasmyth optical table and so would only be used if circumstances demanded and permitted it.

8.3 Camera Enclosure

The camera enclosure will be fitted with several temperature sensors and a dew point sensor. A heating element will be fitted within the enclosure so that the enclosure can be warmed in the event that it is too cold to switch on the camera. Cables associated with these functions will be routed along with the camera cable to Q5, a distance of ~6 m.

8.4 Heat Exchange Enclosure

This enclosure will house the components which are necessary to transfer heat from the camera Peltier cooler and camera enclosure to the EIE-provided cooling circuit. In our conceptual design we expect only a flow valve would be needed to divert the flow of coolant at a suitable flow rate but the nature and amount of electronic control and sensing housed in this enclosure will depend on the amount of heat to be transferred. It is expected that at least one set-point will be sent to this enclosure to control a flow valve or provide a set-point temperature, and that several temperature sensor signals and a flow sensor signal will be returned to the electronics interface.

9 Conceptual Software Design

9.1 Software requirements

The FTT/NAS software will be required as a minimum to accomplish the following tasks, to which we have gives the following names:

1. SystemController: Start up the FTT system, and communicate with the ISS and GUI to receive commands, coordinate their execution, and return status;
2. CameraController: Set up the camera and change its modes;
3. FttaController: Implement the fast real-time control loop which takes high-speed raw sub-frames from the camera, computes and applies an appropriate correction signals on the fast tip/tilt actuator (FTTA);
4. OffloadController: Offload slow corrections from the FTTA to the telescope mount;
5. NasController: Implement the acquisition mode which takes raw full frames from the camera and sends appropriate offsets to the telescope mount (via the ISS);
6. TempController: Provide (slow) real-time control of the camera enclosure temperature (note that real-time control of the CCD temperature is performed by the camera itself) by adjusting chiller parameters;
7. MechController: Control mechanisms (if any) for example to align the system;
8. MonPublisher: Send monitor data to the ISS (and also to the GUI);
9. LocalDataCollector: Optionally record monitor data to a local file for later retrieval;
10. GraphicalInterface: Provide an engineering GUI which allows control of the system and display of status and monitor data.

9.2 Software architecture

The list of tasks above provides a natural partitioning of the software. It has the desirable property that the coupling between partitions is relatively loose, thereby improving the modularity of the code. All of these tasks can in principle run on the same machine, but it would be desirable to have the GUI running on a machine which is directly connected to the console at which it is desired to display the diagnostics, thereby maximising the display bandwidth for real-time video display of the camera frames. Therefore we have adopted a distributed architecture where all the tasks except for GraphicalInterface are executed on the dedicated FTT/NAS computer and GraphicalInterface resides, at least potentially, on a different machine, be it a laptop in the telescope enclosure or the main console in the MROI control room.

Many of the tasks above must be accomplished at roughly the same time and so it is natural to partition them into tasks which can execute in parallel either by sharing a single CPU or through using multiple CPUs, for example in a multi-core processor. Common methods for achieving this parallel operation include:

- Threads, where parallel tasks share a single address space and the operating system takes care of allocating tasks between CPUs and time-slicing each CPU to work on multiple tasks;
- Processes, which are collections of one or more threads which have an address space which is different from other processes and so processes cannot read or write other processes' data directly;
- Event-driven programs, where a single thread switches between multiple tasks based on “events” which typically signal either the availability of a data channel for reading or writing or the timeout of some programmed timer.

Threads have the advantage of being “lightweight” in that it is relatively inexpensive to create thousands of threads on a single machine, but using multiple threads introduces complexity in both programming and debugging because different threads can trample on each other's data. Often complex locking mechanisms are required to ensure non-overlapping access to common data. Care is needed to avoid accidentally overwriting the data of other threads and this requires using thread-safe libraries.

Processes provide more decoupling between tasks, to the level that any process can crash but will still leave the others running. This comes at a price that inter-task sharing of data is more difficult, which can be a problem if high data bandwidths are involved. An advantage of processes is that different processes can run on different machines that are only connected over a network, and it is straightforward to write different processes using different programming languages which are best suited to each task.

Event-driven programs are a form of “co-operative multi-tasking”: each section of a task is written in short-execution-time blocks (“callbacks”) with the (correct) assumption that no other task is accessing any of the data during the execution of that block. However, data can still be shared between tasks. Debugging is easier since there is only ever one task executing at a given time. A problem of event-driven tasking is “inversion of control” in that the order that individual callbacks are executed in depends on the order in which events arrive, rather than being determined by the main program. As a result, writing single long sequential tasks as a collection of sub-tasks becomes more complex, typically involving the use of implicit or explicit state-machines. Event-driven programs also cannot guarantee latency of execution for any task because this depends on the longest time required for any callback to run.

An application can make use of a combination of these methods to implement multiple tasks. We have chosen to split the tasks using the best tasking model for each group of tasks, and this division is shown in Figure 17.

The FTT application would thus be divided into the following processes:

1. A GUI process (task GraphicalInterface): this needs to be able to reside on a different machine, and when the system is running under the control of the ISS the GUI is not required;

Figure 17: A diagram showing the tasks and dataflows within and external to the FTT/NAS software. Items inside ellipses are tasks while the rectangles indicate process boundaries. The FttController and NasController may be implemented as kernel threads but are shown as user-space threads in this diagram. Flows of monitor data from the tasks generating the data to the MonPublisher are not shown in order to not clutter the diagram. We understand that MRO would prefer to route communications between the FTT/NAS software and the AMOS-provided UTCS via the ISS (not directly as shown in the diagram), and we are happy to comply with this.

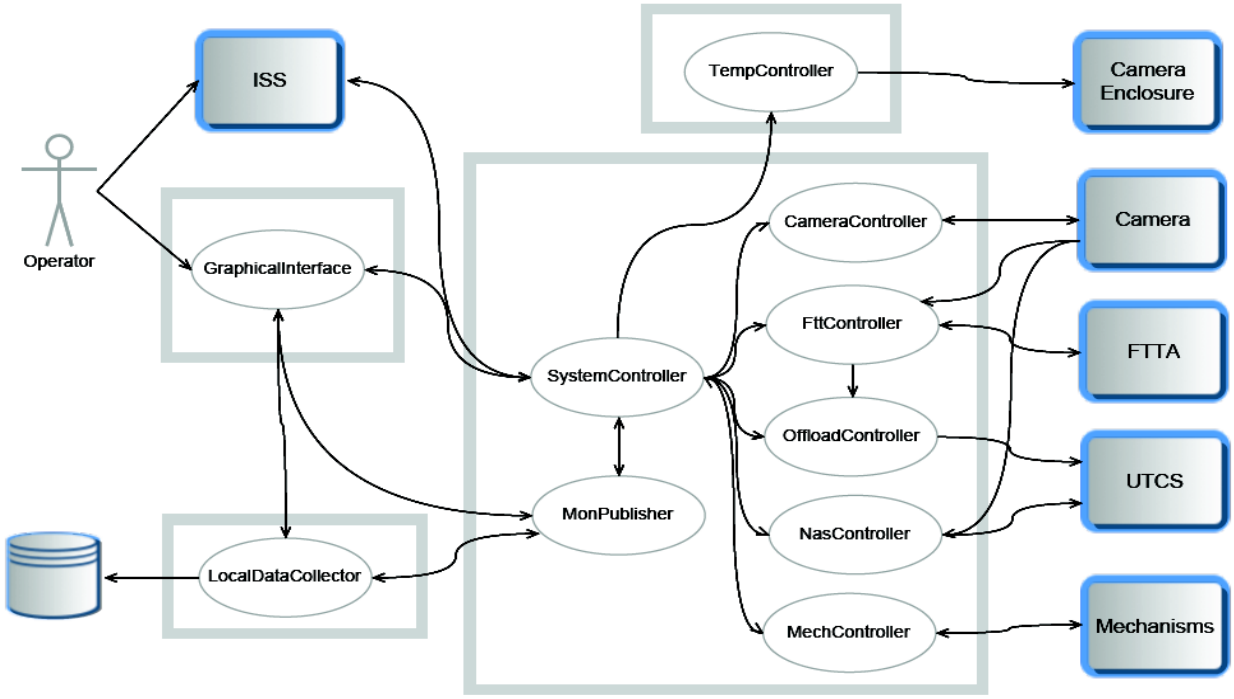

2. The temperature controller process (task TempController): a long-running task which will likely need to operate during the daytime in order to maintain the camera enclosure temperature. It is relatively weakly coupled to the rest of the tasks and needs to share very little common state;

3. A local data collector (task LocalDataCollector): this task is likely to be a copy of the ISS data collector software: it has very similar functionality to the latter, but use of the identical software will require understanding the ISS software in more detail;

4. A Xenomai real-time thread (tasks FttaController and NasController): this task may be a Xenomai kernel thread, but it may also be a Xenomai user-space thread, in which case it would be part of the process enumerated below. This thread handles frames arriving from the camera and performs the FttaController or NasController tasks and is scheduled by a real-time interrupt when the camera frame arrives. Since the FttaController and NasController tasks never run at the same time, switching between the tasks is simply accomplished using a single state variable local to the thread;

5. A master process (all remaining tasks): this collects together tasks which have relatively tight coupling or do not merit a separate process.

The non-Xenomai tasks in the master process could be executed either as threads or as an event-loop. The decision as to which of these to use has not been taken, and depends to some extent on the ISS command API which has both threads and non-threads versions: the final details of this API were not known at the time of writing this document.

For the purpose of describing at least one candidate architecture, we assume that all the remaining tasks are implemented as threads. To avoid problems with conflicting access to shared state, the threads are designed

to use as little shared state as possible, making use of information hiding techniques such as private variables. Instead the threads use the "actor model", where each thread communicates with other threads using a message-passing paradigm. A possible implementation for this is the in-process message queue system provided by "ZeroMQ", an open-source messaging stack (www.zeromq.org).

For communicating with tasks in different processes within the FTT/NA system, the ZeroMQ software can also be used, making use of TCP/IP or Unix sockets. Once the connection has been set up, ZeroMQ makes communication to intra-process tasks look identical to communicating to extra-process tasks. This means that threads can be moved to different processes quite easily, so that the assignment of tasks to threads and processes need not be frozen in stone at an early stage.

9.3 Detailed software design issues

9.3.1 Real-time architecture for the fast tip-tilt system

The fast tip-tilt software must download camera data, calculate an error signal and send correction voltages to the fast tip-tilt mirror in "hard real-time". That is, it must reliably meet a hard deadline (100 µs from the receipt of camera data to outputting a control voltage) for every camera frame. The hard real-time requirement can only be met through running the application in a hard real-time operating system, such as QNX, RT-Linux, or Xenomai, none of which are supported by the candidate camera vendors. However, vendors do often support Linux, which is well integrated with RT-Linux and Xenomai. This raises the possibility of porting the vendor's drivers to one of these operating systems to get real-time response. The Cambridge team has chosen Xenomai because the software is completely open, the licensing fee is zero, and Xenomai has proved itself in the Cambridge team's delay line metrology software development.

A camera software development kit for Linux generally operates as in Figure 18 (a). A camera firstly transmits image data to an interface card on a host computer. The card transfers the data into a pre-allocated region in computer memory, and asserts a hardware interrupt line when it is finished. The Linux kernel notices the interrupt, gracefully stops whatever it is currently doing and starts execution of the camera interrupt service routine. The interrupt service routine reads the image data from the computer memory and sends it to an interface driver, which places it in a buffer that can be accessed from user space. In user space a vendor-provided library handles access to the data and camera control, and presents the user with a programming interface with which they can build their own application.

Unfortunately, in Linux the time between a hardware interrupt and execution of the interrupt service routine (the "interrupt latency") is not bounded[5], which could result in missed deadlines in the fast tip-tilt application. Hence a real-time port becomes necessary.

Any port of the vendor's software to Xenomai should be as non-invasive as possible, to simplify porting of vendor revisions and of any non-real-time software written for the First Light Camera. Additional complications can arise if the software is partially closed-source as this limits the scope for modification. However, it is envisaged (and in one case, demonstrated) that the behaviour will be something like Figure 18 (b).

In this scenario, starlight arrives at the camera via the fast tip-tilt mirror. The camera downloads its data to an interface card, which then writes it to computer memory and triggers an interrupt as before. Xenomai, which coexists with the ordinary Linux kernel, intercepts the interrupt before it gets to Linux, and with bounded latency commences execution of a custom Xenomai interrupt service routine. This interrupt routine has all of the functionality of the original interrupt routine, but additionally calculates and sends a correction signal to an analogue interface card, which converts it into tip-tilt mirror voltages (several analogue cards have been found with sufficiently open architecture that a custom Xenomai driver can easily be written). Hence the servo loop is closed entirely within the Xenomai domain.

[5]The Linux 2.6 kernel can be compiled with the "PREMPT_RT" patch enabled to allow real-time performance. This feature will be exploited in the upcoming Xenomai 3.

Figure 18: A diagram of the operation of the normal Linux driver (a) and the driver modified for closing the real-time loop (b) as discussed in the text.

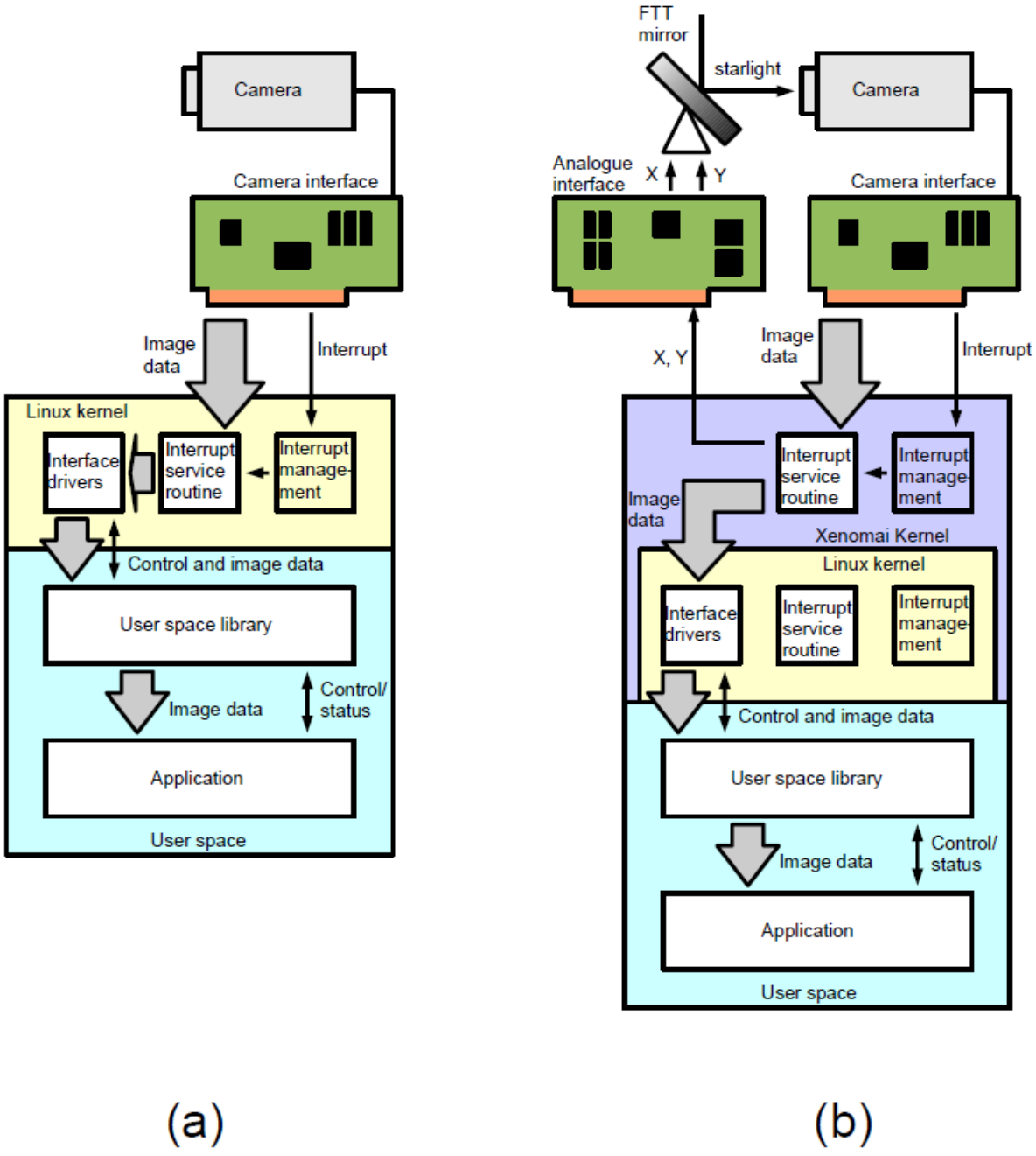

From this point the image data gets passed to the ordinary Linux interface driver, which interacts with the user-space library and application as before. Hence code that makes use of the library, such as that which may be written for the FLC, can be re-used. The ordinary Linux interrupt service routine, while still present, never sees the interrupt that was originally destined for it and remains idle.

The user-space code is able to execute for the remaining ~900 µs (assuming a 1 kHz frame rate in FTT mode) before it is pre-empted by the next frame arriving from the camera. This CPU time is available for all of the non-real-time tasks listed in the previous section, including tasks which alter parameters used by the Xenomai interrupt service routine (such as receiving objective-point offsets from the ISS). The new parameters will therefore be used to process the next camera frame.

This architecture has been shown to work with the Andor iXon^{EM}+897 camera and the Andor Linux software development kit. In this case, the interrupt latency was shown to vary between 16 µs and 32 µs, even on a heavily loaded system. It is also expected to work with Camera Link cameras, as Camera Link vendors often provide open-source Linux drivers or closed-source drivers with enough access to implement real-time schemes.

9.3.2 PCI bus conflicts

The most time-critical real-time task is the FTTA control loop. While the Xenomai kernel will ensure exclusive access to a CPU when the real-time interrupt occurs, conflicts for the PCI bus from other bus controllers have the potential to cause latency problems in getting the camera pixel data transferred to main memory. Such conflicts are most likely to arise from (a) hard-disk DMA traffic and (b) network traffic.

It may be necessary to avoid writing to disk during real-time operation of the FTTA, for example having a mode in the data collector where data is only buffered to memory during FTTA closed-loop operations and written to disk afterwards.

It may also be necessary to explicitly schedule communication with the Ethernet card for the period just following the completion of each real-time interrupt. It may be possible to effect this using the RTnet real-time Ethernet driver in Xenomai. Since the real-time closed-loop calculations take only 100 microseconds of the 1 millisecond interval between interrupts, there is adequate time to schedule such activity, but the issue that would need to be resolved (should network traffic prove to be a problem) is whether access to the card can be controlled by RTnet while allowing normal TCP/IP traffic to the non-real-time tasks to flow over the link.

9.3.3 Programming language

There are a number of factors influencing the choice of programming language. Since the source code is a deliverable of the FTT/NAS work package, then using a language which is well supported at MRO is a key factor. The API to the ISS is available in Java and C, so these two languages are to be preferred. The Xenomai real-time programming interfaces are available in C, and the Cambridge group has experience of delivering software to MRO in C, so C is an obvious choice for programming most if not all of the system. There may be some advantage in using Java for the GUI, if MRO develops a generic display interface for the monitor data, otherwise a C or C++ graphical toolkit such as Gtk or Qt could be used.

9.3.4 First-light camera software

In order to save resources, the FLC software will be as far as possible a strict subset of the FTT/NAS code. A minimum system would consist of a SystemController (only the startup functions and the interface to the GUI are needed), a CameraController, a substantial portion of the NasController, the portion of the MonPublisher to feed data to the GUI, a minimal GraphicalInterface, and a minimal LocalDataCollector. The only LocalDataCollector feature required is that which saves the centroid data, so it may be possible to implement this functionality in the GraphicalInterface. The FLC will need to be temperature controlled so as to protect the camera even though it is not necessary to maintain a low surface temperature differential with ambient. Therefore a TempController will be required for the FLC.

10 Lifetime and maintenance

10.1 Mechanical components

Since there are no moving parts or actuators in our preferred conceptual design, there are no life-time issues for components on the optical table. For parts off the optical table, the only electromechanical item envisaged is the flow control valve which controls the flow rate of cooling fluid to the camera and camera enclosure. This valve will be selected to suit the lifetime requirement and will be a low maintenance component.

10.2 Optical components

The FTT/NAS optical components will be be coated as appropriate but these coatings may need cleaning or replacement after several years given their exposed environment in the UT dome.

10.3 Electronics components

All electronics components, such as PCs and interfaces, will be sourced with lifetime in mind but the availability of replacement parts cannot be guaranteed. The design has been modularised so that replacement of any one component is made easier by not attempting to combine all interface functions on one multi-purpose board.

10.4 Camera

The EMCCD cameras are supplied with a 1 year warranty and possibly a longer warranty on the vacuum seal for the detector chamber. There are no maintenance issues except in keeping the camera window clean and ensuring that there is no corrosion or particulates in the cooling tubes. Faults with the camera or with the vacuum chamber will require the camera to be returned to the manufacturer.

Some lifetime issues with e2v EMCCDs exposed to light at high gain have been reported, and we have assessed the test results published by Andor (`http://www.andor.com/pdfs/Longevity_in_EMCCDs.pdf`). In the worst case we are using the gain register a factor 40 times less intensively than in the Andor test, using a factor 4 less gain. Andor measured a lifetime of 7 years for their very aggressive test and we conclude therefore that there are no lifetime issues for our application.

11 Interfaces

The FTT/NA system interfaces to five major subsystems, and the FLC to four of these (there is no interface from the FLC to the FTTA). These interfaces will be controlled using Interface Control Documents developed by the Cambridge team. Two provisional ICDs already exist as parts of documentation supplied by other vendors (see Table 14). We propose to separate and detail these interfaces in the set of ICDs we develop for the FTT/NA and FLC systems, referring to the source documentation as necessary. Where the content of an ICD is expected to be identical or overlapping for the FTT/NAS and FLC, a single ICD will cover both systems. We have listed separate FTT/NAS and FLC ICDs to the ISS since the FLC is expected to implement only a small subset of the FTT/NAS commands and data streams.

The proposed set of interface documents are listed in Table 14. The expected contents of each ICD are given in RD4.

11.1 Specific Interface issues

Here we have identified a number of critical or urgent interface issues that we believe require assessment in the near term:

ICD reference number	Owner	Description
MRO-ICD-CAM-1100-0108 FTT/NAS-FTTA MRO-ICD-AMO-6000-025 FTTA-FTT	CAM AMOS	Specific FTTA-FTT interface General UT electrical ICD
MRO-ICD-CAM-1000-0109 FTT/NAS,FLC-UTE MRO-ICD-EIE-0032 UTE-FTT	CAM EIE	FTT/NAS & FLC to Enclosure ICD Enclosure to FTT system ICD
MRO-ICD-CAM-1000-0110 FTT/NAS,FLC-NOT	CAM	FTT/NAS & FLC to optical table ICD
MRO-ICD-CAM-1000-0111 FTT/NAS,FLC-UT	CAM	FTT/NAS & FLC to UT optical ICD
MRO-ICD-CAM-1100-0112 FTT/NAS-ISS	CAM	FTT/NAS to ISS ICD
MRO-ICD-CAM-1200-0113 FLC-ISS	CAM	FLC to ISS ICD

Table 14: List of FTT/NAS and FLC interface documents

- Stability of the Nasmyth optical table. This has potential system-wide impact;
- Cooling: we request that cooling loop 1 (EIE electronics housing) rather than loop 2 be routed to Nasmyth optical table [TBC];
- Dry air: we request that air be supplied to the Nasmyth optical table and understand that we should include suitable drying equipment as part of our system;
- The cable route from the FTT/NAS sensor on the optical table to controller in electronics housing: The camera cable is 6 m maximum and the latest calculation of the route it must take is approximately 5.3 m. This should be sufficient margin;
- The FTT/NAS space envelope: we request that parts of AAS be separated to allow a common base-plate to be used for FTT/NAS components;
- Power consumption: we request an increase in FTT/NAS power consumption allowance and a potential increase in power dissipation if an alternative candidate camera must be chosen.

12 CoDR Summary

We have presented our outline of the conceptual design of the MROI FTT/NA system as it currently stands. We believe that a system that meets almost all of the requirements enumerated in the Technical Requirements Document INT-403-ENG-0003 can be delivered, and that where there may be a gap between what is realistically possible and what has been specified in that document, this gap will likely be small. We are confident that the risk of our proposed system being non-compliant with the full set of technical requirements is low, save for a small number of issues (see below).

In the following sections we review in brief our assessment of the technical sufficiency of our concept design under six main areas, and finally summarise how we intend to proceed.

12.1 Optical layout

We are confident that a solution to the optical layout for the FTT/NAS can be realised straightforwardly despite the heavily populated nature of the UT Nasmyth optical table. The particular layout we have focused on most closely is the “dog-leg transmissive” (DLT) configuration, which utilises a relatively compact baseplate, and for which we have already developed preliminary designs for the required optics.

However, the zoom layout, which potentially offers the most mechanically stable configuration of all the FTT/NAS components, remains of high interest. We intend to expedite further exploration of the designs

for positive and negative apochromatic lenses that will deliver a suitably compact PSF at all wavelengths and temperatures of interest as soon as possible.

The most concerning issue regarding the choice of optical layout will be the actual thermally-induced deformation of the Nasmyth optical table when it is integrated into the UT superstructure. Our layouts have all assumed the use of an optical baseplate to mitigate against any differential displacements of the critical optical elements of the system due to deformations of the optical table, but the extent to which this will meet the overall MROI top-level system design goals remains to be seen.

12.2 Camera selection

Of the three potential candidates for the FTT/NAS sensor, the Andor iXon^{EM}+897 camera appears to be the lowest risk choice. Our one remaining concern is that the vendor has yet to come back to us to confirm that a custom 23 $\times$ 23 pixel fast readout mode can be guaranteed. We intend to expedite closing this uncertainty by paying for the necessary custom software development in the near future. Of the remaining cameras both have their pros and cons. The use of the Princeton Instruments ProEM 512B camera is a possible fallback strategy, but there are real uncertainties associated with the time-line for real-time Linux support becoming available and a concern about how much heat it may dissipate. The Hamamatsu ImagEM C9100-13 camera – which we did not test in the lab – is the least well characterised possibility. It appears to have the poorest low-temperature survival capability but in other areas, e.g. software support, appears suitable.

It seems clear that the sooner we can confirm the suitability of the Andor iXon^{EM}+ 897 head, the better. This will be a high priority task for us in the near term.

12.3 Opto-mechanical design

The very challenging derived requirements on the stability of the optical components of the FTT/NA system have been mentioned multiple times within this document. Our strategy for realising the necessary stability will be to use simple symmetric mounting arrangements so as to minimize the effect of any induced thermal gradients when the ambient conditions alter. We also plan to reject any schemes that include adjustable elements as integral parts of the mounts, since these are likely to creep in non-repeatable ways in the exposed environment in which the FTT/NAS must be located. With these design assumptions our FEA studies have made us confident that stability at or very close to the required level can be realised using aluminium components. Any differential expansion effects with respect to the steel top of the optical table will lead to an effective shear of the FTT/NA system in the vertical direction with respect to the input beam from the UT which is not a show-stopper.

A more serious concern is the fact that in all the proposed layouts the FTT/NAS sensor must sit on the Nasmyth table (and not the optical baseplate) and so the stability of the table itself becomes a critical issue. The Technical Requirements Document allows for any table-induced instabilities to be ignored for the purposes of system performance verification, but we believe it will nevertheless be prudent for us to further investigate the Zoom layout since this permits the camera to be positioned as close as possible to the baseplate. This is one approach to help mitigate the effects of table deformation and we have borne this possible problem in mind throughout our opto-mechanical design.

If however a large-magnitude large-scale deformation of the table occurs when the temperature changes by a few degrees Celsius this could lead to an overall tilt of the baseplate on which we intend to mount the optical components. In turn this might result in the desired zero-point stability not being achievable. Appendix A presents some preliminary calculations for the magnitude of this type of effect. We would wish to draw these preliminary calculations and the identification of a potential system problem to the Project Office's attention at this moment in time.

12.4 Thermal design

If we are able to utilise the Andor iXon^{EM}+ 897 camera head, we are confident that all thermal issues will be relatively straightforward to address. We will tap into the EIE-provided coolant loop used for the electronic enclosures and this will be sufficient to meet the system needs. We also expect that meeting the 250 W total power dissipation requirement will not be a problem.

If one of the other camera systems is utilised, then this could be problematic. Not only will the additional heat from the head need to be dissipated, but the power required for the heads and ancillary electronics will be higher by roughly 100 W. These are unlikely to be show-stoppers, but will require additional design work and implementation effort.

12.5 Electronics design

We have no reason to believe that the electronics needed for the FTT/NAS will be a problem to deliver. We have assessed that there is sufficient rack space for these and that the total power budget is compliant with what can be realised.

12.6 Software design

As for the electronics hardware above, we do not see any critical issues related to providing suitable hard-real time and non-real time elements of the software needed for the FTT/NA system. Unless we are forced to use the ProEM 512B camera head, we do not assess this to be a high risk area, and will aim to capitalise on our experience with the MROI Delay Line software and our initial tests and investigation of various open-source software components. If the ProEM 512B camera must be used, the associated risk will be one of time and possible schedule delays rather than software technical non-compliance.

12.7 Conclusions and route forward

In conclusion, we believe that our initial investigations, studies and analyses suggest that we have a viable concept for delivering the MROI FTT/NA system in a way that is broadly speaking compliant with the Technical Requirements Document (see RD5 for the complete compliance matrix). However, we have identified a number of key risk areas that will need to be quantified, assessed, and, if necessary, mitigated as a matter of urgency. These can be summarised as follows:

- **Camera selection:** As has been made clear above, the final down-selection for the FTT/NAS sensor head has still to be made. We believe that the Andor iXon^{EM}+897 camera is the preferred choice but until we have confirmed that a custom 23×23 pixel fast readout mode can be guaranteed an uncertainty remains. If either of the other two possible cameras must be used, there will likely be a greater amount of design, prototyping and test work involved in the project;
- **Opto-mechanical stability:** We are confident that we can meet – or get very close to meeting – the necessary stability requirements for the optical elements of the FTT/NA system. This confidence is based both on our FEA and other analytical results and our experience of similarly stringent opto-mechanical projects. The level of imprecision in our assessment is roughly a factor of two, i.e. if the requirement to keep an optic stable in position is 0.5 microns, we are confident that we realise a stability between 1 and 0.5 microns. Similarly for a stability requirement in angle of 1/20th of an second of arc, we would expect to reach a stability of between 1/10th to 1/20th of a second of arc. This uncertainty is related primarily to the inherent difficulty in predicting exactly what temperature inhomogeneities are likely to obtain within the populated UT enclosure. These cannot be modelled at present in any reliable way, and so mitigating this uncertainty may be problematic.

- **Nasmyth optical table stability:** Perhaps the most important result of our conceptual design work has been the identification of the potential for the Nasmyth optical table to provide a hard limit to the stability of the FTT/NAS zero-point and to the efficacy of a once-per-night alignment process. While the management of the stability of the Nasmyth optical table goes well beyond the scope of the FTT/NAS contract, the mitigation of its impact has been addressed in some of our design tasks. However, we recommend that the MROI Project Office assess this risk from a system-wide point if view as soon as possible, so that the ramifications of any mitigation strategy on the FTT/NA system design can be studied as early as possible;
- **Impact of speckle noise:** We have yet to fully analyse the impact of uncorrected instantaneous PSF perturbations (i.e. polychromatic speckle noise) on the precision and accuracy to which we will be able to measure the centroids of the FTT/NAS target images. We do not expect this to lead to a significant signal-to-noise penalty and we have included a "median-case" contribution for it in our analyses. However, it remains as a small additional uncertainty. We are developing a numerical simulation to verify our estimate for its impact now;
- **Limiting sensitvity:** Our derived requirement calculations suggest that it will not be possible to reach a limiting sensitivity of $m_v = 16$ under the assumptions defined in the Technical Requirements Document. To do so would require a throughput >100% from the UT to the FTT/NAS sensor window, a figure which is clearly unreasonable. We believe that a more realistic sensitivity limit is $m_v = 15.8$. This figure can be expressed in an alternative, and perhaps more useful manner, by saying that at $m_v = 16$ we calculate that the residual two-axis tip-tilt jitter will not be 0.06 seconds of arc but be roughly 2% over-budget instead. Thus, this limit to sensitivity should not be seen as a show-stopper but rather as a slight degradation of the systems performance at the very lowest light levels. More precisely, there will be an additional 0.5% visibility loss in the H band over what has been allocated in the interferometer visibility loss budget at $m_v = 16$;
- **Dynamic range:** Our current concept design, which assumed a limited number of gain settings for the FTT/NAS sensor can only accommodate targets as bright as magnitude $m_v = 3$. Although the need to observe brighter targets is not an explicit system requirement, if it is desired to operate with brighter targets additional hardware to attenuate the incoming starlight will need to be designed and installed.

Closing down on as many of these as possible will be the next major element of our design work.

A Thermal modelling details

The parameters used for the thermal model were estimated using suitable approximations for the volumes and masses of the camera and enclosure, the areas of cold plates, a fluid coupling area for typical cold plates, the properties of air at a height of 3 km and a cooling fluid of water and glycol in a 50:50 ratio. Heat transfer coefficients were calculated for each surface arrangement and an average value used. Expressions and values for the model parameters are tabulated below.

A.1 Evaluation of thermal model parameters

Thermal capacitances for the model are evaluated and presented in Table 15. These are included in the model so that time constants can be investigated if desired but do not affect the steady-state heat transfer.

Thermal resistances for the model are evaluated and presented in Table 16. Convective heat transfer coefficients were calculated at the mean temperature differences for the camera to internal air, the internal air to enclosure wall, the internal air to cold plate and the external air to enclosure surface. The radiation heat transfer coefficient was based on a linearisation of the relationship at 278 K. The conductivity of the enclosure insulation is a typical value for the "aerogel" products currently available. The mass flow rate and specific heat of the fluid are typical

Thermal capacitance	Formulae	Evaluation
Camera	$C_c = V_c \rho_{ss} c_{pss}$	$2 \times 460 = 920$ J/K (use 2 kg of stainless steel)
Enclosure air	$C_e = \rho_{air} c_{pair} V_{enc}$	$0.942 \times 1007 \times 0.016 = 15.2$ J/K
Cold plate	$C_p = \rho_{al} c_{pal} V_p$	$2698 \times 917 \times 0.0003 = 742$ J/K
Cooling fluid	$C_f = \rho_f c_{pf} V_f$	$91 \times 3350 \times 2.3 \times 10^{-5} = 70$ J/K (50% water/glycol)

Table 15: Evaluation of equivalent thermal capacitances.

values one might use but significant changes to these have little effect on the heat removed because the largest thermal resistance is between the internal air and cold plate.

The convective heat transfer for the outer surface of the enclosure assumes normal convection, i.e. not driven by airflow changes due to wind, and as such it is a worst case scenario.

Thermal Resistance	Formulae	Evaluation
Camera-air	$R_{ce} = 1/h_{cce} A_c$	h_{cce} = 4 W m^{-2} K^{-1} (average of all surfaces and ΔT=20 °C) giving $1/(4 \times 0.112) = 2.2$ K/W
Plate-air	$R_{pe} = 1/h_{cpa} A_p$	h_{cpa}= 2.9 W m^{-2} K^{-1} (average of all surfaces and ΔT=8 °C) giving $1/(2.9 \times 0.3) = 1.15$ K/W
Plate-fluid	$R_{pf} = 1/h_{cpf} A_f$	h_{cpf} = 100 (estimated) giving $1/(100 \times 0.015) = 0.66$ K/W
Insulation	$R_{ins} = L_{ins}/k_{ins} A_{os}$	L_{ins} = 40mm conductivity k_{ins} = 0.02 giving $0.04/(0.02 \times 0.4) = 3$ K/W
Fluid	$R_i = 1/m'_f c_{pf}$	Equivalent Thermal Resistance representing heat loss due to temperature difference and mass flow rate m'_f and specific heat of fluid $c_{pf} = 1/(0.015 \times 3.35e3) \sim 1/50 = 0.02$ K/W
Internal surface-air	$R_{if} = 1/h_{cif} A_{is}$	$h_{cif} = 2.3$; assume ΔT ~ 2 °C; $L_c = 0.29$; $R_{if} = 1/(2.3 \times 0.36) \sim 1.2$
External surface-air	$R_{of} = 1/h_{cof} A_{os}$	h_{cof} = 2; assume ΔT ~ 2 °C; $L_c = 0.29$; $R_{of} = 1/(2 \times 0.64) \sim 0.78$
Radiation	$R_{or} = 1/h_{ros} A_{os}$	$R_{or} = 1/[F_e \cdot F_a \cdot A_{os}(T_1^2+T_2^2)(T_1+T_2)] = 1/0.8 = 1.25$ for T_1 = 280 K and T_2= 278 K. F_e assumes surface emissivities of 0.7 and F_a is an average shape factor.

Table 16: Evaluation of equivalent thermal resistances.

B Nasmyth Optical Table Analyses

The aim of the following FE analyses is to determine the temperature difference between the air above and below the Nasmyth table that would lead to a tilt of 0.047″ of the table surface at the position of the dichroic mount. This is done in two stages: (a) finding the difference in temperature between the skins of the optical table which will produce the tilt and (b) by finding the air temperature difference which produces the skin temperature difference.

B.1 Optical table bending calculation

The purpose of this analysis was to calculate the tilt of components mounted directly to the optical table under the condition that there are different temperatures on the top and bottom skins. An estimate of the tilt of a base-plate can be obtained from these data if the displacements of the table surface at the baseplate interface points can be calculated.

The assumptions made for the analysis were:

1. That the same material has been used for the top and bottom skins of the table;
2. That the bending of the table is in spherical geometry;
3. Than the deformation of the table from the table support is assumed insignificant (i.e. it has been ignored);
4. That the tangent plane to the table surface at the centre of the table remains horizontal.

The equation for bending is based on the deflection of an I-beam subject to differing temperatures between the top and bottom of the beam. In this case

$$\theta = W \times \Delta T \times k/h \,, \qquad (1)$$

where θ is the angle that the two points on the table make with each other, W is the distance between the two points, ΔT is the temperature difference between the top and bottom table skins, k is the CTE of the table surface material, and h is the thickness of the table.

The tilt of the dichroic optic on the bending surface is shown schematically in Figure 19.

There are two coordinate systems here which are *O-XYZ* and *O'-X'Y'Z'*. *A'* represents the centre on the top surface of the optical table. The *X'OY'* plane is horizontal. The optic seats vertically on the table surface at position *A* with a tilt angle γ which is the angle between its surface and the *Y* direction. The optical component is initially in coordinate system *O-XYZ*. The coordinate system becomes *O'-X'Y'Z'* after rotations in *X* and *Y* of θ_x and θ_y. The aim is to calculate the angle which the tangent at the surface of the table at point *A* now makes with respect to the tangent to the surface at the centre of the optical table. The change in tilt of the optical component will be equivalent to this angle. The transformation between the two coordinate systems can be written as:

$$\begin{bmatrix} X' \\ Y' \\ Z' \end{bmatrix} = \begin{bmatrix} 1 & 0 & 0 \\ 0 & \cos\theta_x & -\sin\theta_x \\ 0 & \sin\theta_x & \cos\theta_x \end{bmatrix} \begin{bmatrix} \cos\theta_y & 0 & \sin\theta_y \\ 0 & 1 & 0 \\ -\sin\theta_y & 0 & \cos\theta_y \end{bmatrix} \begin{bmatrix} X \\ Y \\ Z \end{bmatrix},$$

which can be simplified to:

$$\begin{bmatrix} X' \\ Y' \\ Z' \end{bmatrix} = \begin{bmatrix} \cos\theta_y & 0 & \sin\theta_y \\ \sin\theta_x \sin\theta_y & \cos\theta_x & -\sin\theta_x \cos\theta_y \\ -\sin\theta_y \cos\theta_x & \sin\theta_x & \cos\theta_x \cos\theta_y \end{bmatrix} \begin{bmatrix} X \\ Y \\ Z \end{bmatrix}.$$

Since $\boldsymbol{i}$, the unit vector normal to the surface of the optical component, is given by $[-\cos\gamma, \sin\gamma, 0]$ in the *O-XYZ* frame, in the *O'-X'Y'Z'* co-ordinate system it becomes:

$$\begin{bmatrix} X'_n \\ Y'_n \\ Z'_n \end{bmatrix} = \begin{bmatrix} -\cos\theta_y \cos\gamma \\ -\sin\theta_x \sin\theta_y \cos\gamma + \cos\theta_x \sin\gamma \\ \sin\theta_y \cos\theta_x \cos\gamma + \sin\theta_x \sin\gamma \end{bmatrix}.$$

Figure 19: Diagram of coordinate systems used in optical table bending calculations

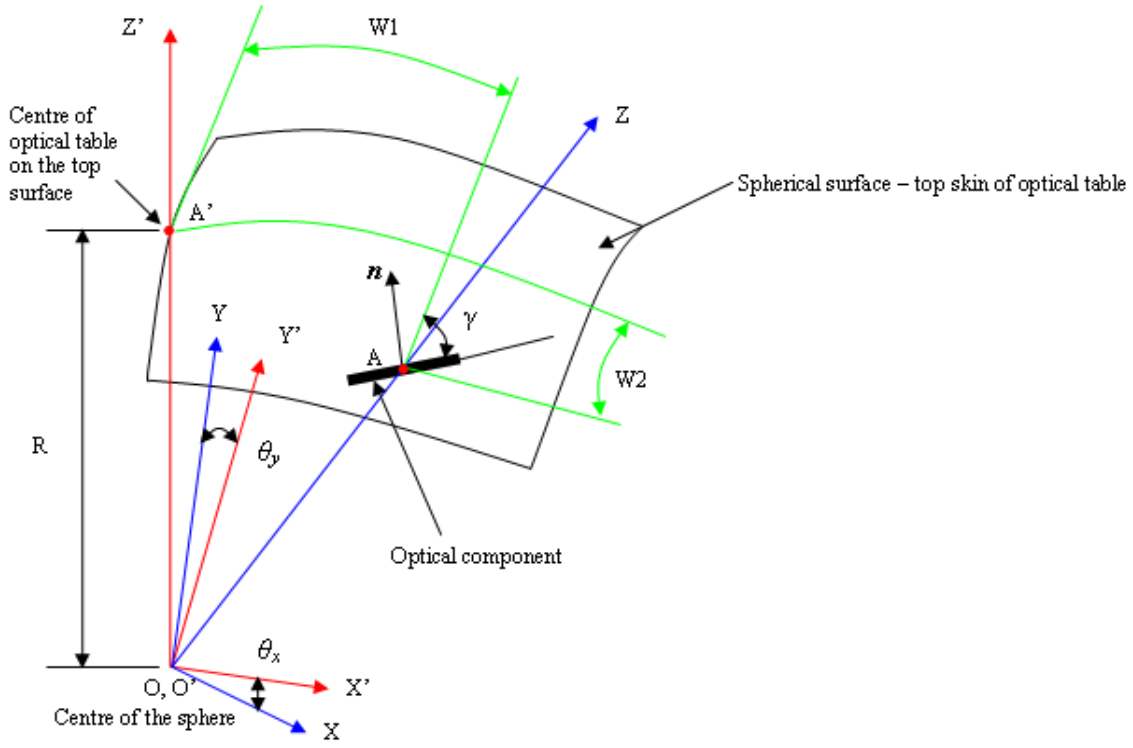

The angle of tilt that $\boldsymbol{i}$ makes with the $X'O'Y'$ plane, ϕ_{tangent} can then be derived as:

$$\phi_{\text{tangent}} = \frac{\sin\theta_y \cos\theta_x \cos\gamma + \sin\theta_x \sin\gamma}{\sqrt{(-\cos\theta_y \cos\gamma)^2 + (-\sin\theta_x \sin\theta_y \cos\gamma + \cos\theta_x \sin\gamma)^2}} . \qquad (2)$$

B.1.1 Case study for the dichroic position

In this case the relevant distances are W1 = 400 mm; W2 = 300 mm; and γ is 75 degrees.

The thickness of the optical table is 112 mm and the skin material for the top and bottom surfaces is stainless steel which has a CTE of 16×10^{-6} /°C.

If the temperature difference between the top and bottom surfaces of the table is 0.01 degrees, then from equation (1): θ_x equals 5.71×10^{-7} radians and θ_y equals 4.29×10^{-7} radians.

From equation (2) the tilt of the dichroic is 6.6×10^{-7} radians or 0.14 arc seconds.

From Table 3 the permitted tilt of the dichrioc is 0.047 arc seconds, which is 1/3 of this value and therefore the temperature difference of the skins is 1/3 of 0.01 °C or 0.0033 °C (assuming linear behaviour with temperature over this small range).

B.2 Finite-Element Analysis of Nasmyth Optical Table

To find what air temperature difference might result in a 0.0033 °C difference in optical table skin temperature a thermal FEA was performed using approximate dimensions of the cell structure of the Nasmyth table. It was assumed that there would be no airflow around the Nasmyth table leading to a heat transfer coefficient of approximately 0.5 W/m^2-K.

The size of the hexagon honeycomb cell was calculated based on (i) the dimensions and weight of the optical table (from AMOS document MRO-TRE-AMO-0000-071); (ii) the thickness of the steel sheet (from Newport

table specifications) and (iii) the thickness of the table skins (also from Newport). The precise details of the inner structure of the table are not known but a 43 mm cell size was assumed (Figure 20), which seems reasonable given the known hole spacing on the table surface.

The results are shown in Figure 21. The air temperatures differ by 0.031 °C on both sides of the table when the temperature difference between the top and bottom skins of the table is 0.0033 °C. We note, however, that under calm conditions the air temperature gradient in the telescope enclosure might be significantly different and less favourable. This would lead to potentially higher skin temperature differences and a greater degree of bending.

The thermal conductivities used for the FEA were:

- Epoxy 0.35 W/m-K;
- Stainless steel 16.2 W/m-K;
- Steel 46 W/m-K;
- Air 0.0257 W/m-K.

The boundary conditions used for the FEA were:

- An air temperature of 0.031 °C on the top face of the table;
- An air temperature of 0 °C on the bottom face of the table;
- A heat transfer coefficient for both surfaces of the table of 0.5 W/m^2-K corresponding to no air-flow.

B.2.1 Case study for the three positions of a base-plate

Similar calculations were performed for the locations of the three supports for the common base-plate of the DLT layout and for the location of the camera mount. It was found that for a temperature difference of 0.0033 °C between the upper and lower surfaces of the optical table, the resulting tilt of the dichroic when mounted on the base-plate is 0.02 arcsec. This is a factor of approximately 2.4 better than when the dichroic is mounted directly on the table, where a tilt of 0.047 arc seconds is expected.

For the same conditions the vertical shear of the camera relative to the centre of the optical table is -110 nm. To get a feel for how this compares to the position of the beam centre from the tilted base-plate it is assumed that all of the tilt leads to a vertical deflection at the camera. The distance that the beam moves up is given approximately by twice the tilt of the dichroic multiplied by the focal length of the lens, i.e. a displacement of: 0.04 arcsec $\times$ 4.85 µrad/arcsec $\times$ 1500 mm = 2.91 $\times$ 10^{-4} mm = 291 nm.

The total displacement of the beam centre at the camera is then 291 nm + 110 nm = 401 nm.

This should be compared to a total displacement of 684 nm + 110 nm = 794 nm that would result if a base-plate were not used.

We conclude that using a base-plate reduces the error due to table bending by a factor of two and so is certainly worth having as part of the baseline mechanical design. However the magnitude of the bending-induced errors is still dependent on the exact thermal equilibrium of the table and thus to be confirmed.

Figure 20: Honeycomb structure assumed for the FEA of the Nasmyth Optical Table.

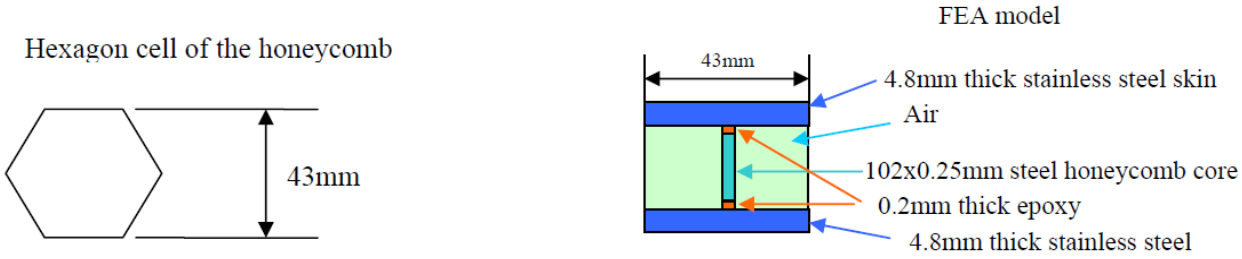

Figure 21: Nasmyth table FEA results. The diagram shows a thermal FEA of the cross section of a cell wall of the table as shown in Figure 20. The stainless steel surfaces are at the top and bottom with a thin steel membrane connecting them. The temperature distribution in the air is very apparent and the difference in temperature of the surfaces is approximately 0.0033 °C.